Institute of Space and Aeronautical Science, University of Tokyo
Report No. 460, March 1971

An Aerodynamic Study of Hypersonic Heat Shielding Problem with Local Mass Injection at Multiple Stations

By

Hirotoshi KUBOTA*

Summary: A study of an axisymmetric laminar boundary layer flow with local coolant mass injection at multiple stations is made by use of an appropriate numerical approach on the basis of the Hartree-Womersley method. The essential feature of the problem consists in discontinuous boundary conditions associated with the local blowing.

In order to check the accuracy of the H-W method applied to the partial differential equations of parabolic type with discontinuous boundary conditions, one-dimensional heat conduction equation is solved numerically as a simple example under the boundary conditions involving several modes of discontinuity and the results are compared with analytical ones. It is shown that the H-W method is applicable if an appropriate difference method is chosen for each mode of the discontinuity. Based on these arguments, an appropriate difference method is presented for an isothermal and an adiabatic wall conditions.

Estimation of cooling effectiveness due to mass injection parameters such as total mass flow and geometrical configurations of coolant mass exit gives the following results;

(1) in order to increase the overall effectiveness of coolant mass injection, the second injection should be located in the upstream vicinity of the peak point of the adiabatic wall temperature or the heat transfer distributions,

(2) if the total mass flow is kept constant, the width of coolant mass exit has negligible effect on the overall effectiveness pertinent to the heat transfer reduction.

An experiment made under the adiabatic wall conditions indicates fairly good qualitative agreement with the numerical results.

Finally, it is suggested that, under the condition of constant coolant mass flow, the effectiveness of the local mass injection cooling is superior to the transpiration cooling.

SYMBOLS

A	area of coolant injection exit
C	Chapman-Rubesin number
Cp	specific heat at constant pressure
d	width of coolant injection exit
E	square error in two-point boundary value problem
H	total enthalpy function

* Research engineer in the National Aerospace Laboratory.
This work was accomplished as the Doctor Thesis while the author was a postgraduate student in the Institute of Space and Aeronautical Science, University of Tokyo.

M_∞ free stream Mach number

$\dot{m}$ mass injection rate

N $= \dfrac{\{2\gamma M_\infty^2-(\gamma-1)\}^{1/4}\{(\gamma-1)M_\infty^2+2\}^{1/4}}{(\gamma+1)^{1/2}M_\infty^{1/2}}\varepsilon^{1/2}\left(\sqrt{\dfrac{8\varepsilon}{3}}\dfrac{1}{1+\lambda}\right)^{-1/2}$

Pr Prandtl number

p pressure

Q total heat transfer

$-\dot{q}$ heat transfer rate

R universal gas constant

R_b radius of body curvature

Re Reynolds number

r_0 cylindrical radius of body

(s, η) transformed coodinates system

T temperature

t time

(u, v) components of local velocity vector

W $= \dfrac{\bar{u}^{2*}}{\bar{C}p_{a_{ir}}\bar{T}_{st}} = \dfrac{8\varepsilon}{3}\left(\dfrac{1}{1+\lambda}\right)^2 M_\infty^2(\gamma-1)\left(1+\dfrac{\gamma-1}{2}M_\infty^2\right)^{-1}$

$\dot{W}$ total mass flow

(x, y) orthogonal coodinates system

x_T transpired length

x_1, x_2, x_3 end-point of mass injection exit

γ ratio of specific heats for air

δ_j boundary layer thickness

θ temperature in one-dimensional heat conduction equation

$\bar{\theta}$ position of the second injection exit

H_c cooling effectiveness for isothermal wall case

κ coefficient of thermal conductivity

Λ_c cooling effectiveness for adiabatic wall case

μ coefficient of viscosity

ϕ transformed stream function

Ψ stream function

ψ transformed enthalpy function

Subscripts;

air conditions of air

c critical condition

e conditions at outer edge of boundary layer

f conditions of the first injection

L conditions with local mass injection

no conditions without injection

s conditions of the second injection

sh conditions just aft of shock wave

st stagnation conditions in free stream
T conditions with transpiration
w conditions at wall
∞ conditions in free stream

Superscripts;

$(\bar{\ })$ properties with dimensions
$*$ reference conditions for non-dimensionalization
$(\ )'$ differentiation with respect to argument

1. Introduction

One of the problems arising from hypersonic reentry of a space vehicle into atmospheric environment is to keep the vehicle structure at a reasonable temperature against the severe aerodynamic heating.

The recent studies have clarified that the form of effective heat-shielding is a coolant gas transfer into the free stream from the surface of the vehicle. It has the advantages that the coolant at low temperature reduces the overall stream temperature near the body surface and increase of boundary layer thickness together with change in temperature profile across boundary layer reduces the heat transfer to the body surface. Moreover, in the case of inhomogeneous mass injection, the effects of coolant molecular weight, specific heat and latent heat of chemical reaction in the boundary layer, etc. contribute to the further heat transfer reduction.

Since the local heating becomes severe in the vicinity of stagnation point of an axisymmetric blunt nosed body, large mass injection at that point, which influences even the bow shock wave, was investigated experimentally by McMahon [*1*], Warren [*2*], etc. Furthermore, it is known from experimental viewpoint that less mass injection separates the boundary layer into two layers, the comparatively thin inner layer in which the temperature is kept almost constant and the outer layer which connects the external properties with inner ones. Libby made the analytical studies by use of this flow model for air [*3*] and helium injection [*4*]. Similar analyses have been recently developed by Fernandez et al. [*5*], Derienzo [*6*], etc. by means of analytical continuation of asymtotic expansions of physical properties in each layer at the interface. Many investigations indicate that the mass injection at the stagnation point is fairly effective on reducing the heat transfer. However, in these cases, the influence of the injection is limited to rather narrow domain and distribution of the adiabatic wall temperature or heat transfer rate has peak point in the downstream region.

Film cooling, transpiration cooling, etc. aim at extending the cooling effect over the wide range by injecting or transpiring a small amount of coolant out of several injection slots or porous surface. These concepts have been discussed especially in the internal fluid mechanics. For instance, Laganelli [*7*] proposed a unified approach to estimate the cooling effectiveness and compared the effectiveness of the film cooling with one of the transpiration cooling. He proposed the results that

the transpiration cooling is more effective process than the film cooling if the mass flow rate is same in both cases, and that the effectiveness of the film cooling approaches to that of the transpiration cooling as the number of injection slots increases.

From the outset of 1960, methods of the film cooling and the transpiration cooling have had a new understanding of the cooling means for a blunt nosed body surface during reentry flight, so that surface heat transfer over a range from the stagnation point to the downstream one was estimated by the help of similar solution of boundary layer equations. Gollnick, Jr. [*8*] showed that the transpiration of air and helium is enough for practical use to cool the axisymmetric stagnation region. Goodwin and Howe [*9*] showed that, in the range of coolant mass flow rate relatively small, the aerodynamic heating is shielded to a great extent and the most effective mass flow rate is from 0.1 to 1.0% of that of free stream.

Ablation cooling is taken to be more effective cooling method. It consists in that the body surface may be melted or sublimated to absorb a part of the heat input into latent heat of phase change. This effect together with that of the mass transfer can reduce the aerodynamic heating considerably. Theoretical study of the ablation cooling has been made in many references [*10*], [*11*], [*12*], [*13*]. However, in spite of a number of advantageous attributes of this method, it has, in structural and economical sense, a defect due to the use of high-polymer materials or graphite as ablators, since it is necessary to renew the eroded surface materials for repeated use of the space capsules.

In consequences, in the future when the frequency of space navigation is expected to increase, any optimum cooling system which makes up for disadvantages of the defect mentioned above should be designed from the technological viewpoint by taking cooling effectiveness, economization and structural safety into consideration.

For this purpose a method of "local mass injection cooling at multiple stations" has been reevaluated recently. This is done in such a way that a small amount of coolant gas is injected into the boundary layer through narrow slits at several stations on the surface, making discontinuous injection distribution.

Localization of the injection stations causes essentially non-similar boundary layer flow and makes the analytical approach very difficult because of the discontinuous boundary conditions. Pallone [*14*] first solved this problem theoretically under the assumption that the boundary layer thickness, surface temperature, mass, momentum and energy are continuous at both sides of discontinuity. In his analysis, although the matching at the discontinuity was treated properly, the extra parameters so introduced were considered as a function of the streamwise coordinate and, consequently, the analysis could be applied only in the neighborhood of the discontinuity. On the other hand, Rheinboldt [*15*] solved a discontinuous suction on a circular cylinder. However, this solution seems to require too complicated mathematical formulation to be applied easily to general problems.

On the other hand, numerical approaches to this problem have been developed by use of high-speed electronic computer. These approaches seem, in principle, to be divided into two methods. The one is the integral method [*16*], [*17*], [*18*].

Especially, Bethel [*18*] applied Galerkin-Kantrovich-Dorodnitsyn method to the boundary layer equations and discussed the convergency of solutions and degree of approximation. Another is Hartree-Womersley method [*19*]. In general, finite-difference approach is constructed either by explicit difference method or by implicit one, and the H-W method corresponds to the improved implicit difference method. The explicit difference method is conditionally unstable, so that mesh size is limited to obtain a stable solution and, therefore, the approximation is not accurate. On the contrary, the implicit difference method has no difficulty on stability and the solution as accurate as is desired may be obtained.

This method was applied to the equilibrium flow around a blunt nosed body in a series of studies by Smith et al. [*20*], [*21*], [*22*], [*23*], [*24*], to the non-equilibrium flow by Blottner [*25*], Fay [*26*], etc., and to the heat transfer problem on the flat faced body by Marvin [*27*].

The H-W method requires to divide the calculated region into several vertical strips despite of the rectangular mesh of the usual finite-difference method. The most important problem appears in adaptability of this method to the discontinuous boundary conditions, because the stability of the solution is assured in the sense of the implicit difference. In this sense, although non-similarity in the flow field and the difference form may be properly treated and the capability of application to the various interesting subjects may be suggested in the references above, the discussions on adaptability of the H-W method applied to discontinuous boundary conditions do not seem to be exact.

This paper presents a numerical approach to local mass injection cooling at multiple stations. The main purpose of the present study is to clarify the capability of optimizing the overall cooling effectiveness with respect to several cooling parameters such as coolant mass flow and coolant slots geometry, etc. Although the numerical method may be essentially based on the H-W method, a reasonable form of difference adaptable to the discontinuous boundary conditions associated with the local mass injection is presented and the two-point boundary value problem is so improved as to give a more general method of approach and faster convergency of the iteration.

2. Fundamental Equations and Free Stream Conditions

A characteristic flow pattern under consideration is shown in Fig. 1, and the essential assumptions imposed on the flow field are as follows;

(1) boundary layer thickness is very small compared with the body radius,
(2) constant density in shock layer,
(3) no chemical reaction, radiation, ionization and dissociation in boundary layer.

In the case that the injected coolant gas is homogeneous, the fundamental equations for the compressible, steady, laminar boundary layer are written [*28*] as

$$\frac{\partial(\bar{\rho}\bar{u}\bar{r}_0)}{\partial\bar{x}}+\frac{\partial(\bar{\rho}\bar{v}\bar{r}_0)}{\partial\bar{y}}=0, \tag{2-1}$$

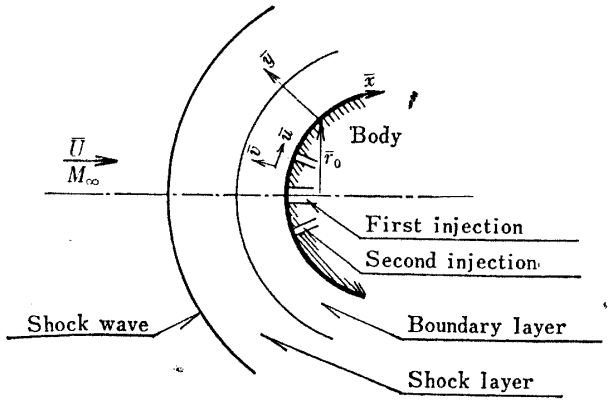

Fig. 1. Characteristic diagram of flow pattern and injection form.

$$\bar{\rho}\bar{u}\frac{\partial\bar{u}}{\partial\bar{x}}+\bar{\rho}\bar{v}\frac{\partial\bar{u}}{\partial\bar{y}}=-\frac{\partial\bar{p}}{\partial\bar{x}}+\frac{\partial}{\partial\bar{y}}\left(\bar{\mu}\frac{\partial\bar{u}}{\partial\bar{y}}\right), \tag{2-2}$$

$$\bar{\rho}\frac{\bar{u}^2}{\bar{R}_b}=\frac{\partial\bar{p}}{\partial\bar{y}}, \tag{2-3}$$

$$\bar{\rho}\bar{u}\frac{\partial\bar{H}}{\partial\bar{x}}+\bar{\rho}\bar{v}\frac{\partial\bar{H}}{\partial\bar{y}}=\frac{\partial}{\partial\bar{y}}\left[\frac{\bar{\mu}}{Pr}\frac{\partial\bar{H}}{\partial\bar{y}}+\bar{\mu}\left(1-\frac{1}{Pr}\right)\frac{1}{2}\frac{\partial\bar{u}^2}{\partial\bar{y}}\right], \tag{2-4}$$

where $\bar{H}$ is total enthalpy and has a form

$$\bar{H}=\bar{C}p\bar{T}+\frac{1}{2}(\bar{u}^2+\bar{v}^2), \tag{2-5}$$

which is reduced, within the accuracy of the boundary layer approximation, to

$$\bar{H}=\bar{C}p\bar{T}+\frac{1}{2}\bar{u}^2. \tag{2-6}$$

The equation of state for a perfect gas is

$$\bar{p}=\bar{\rho}\bar{R}\bar{T}. \tag{2-7}$$

By introducing non-dimensional expressions

$$\left.\begin{aligned}
&x=\frac{\bar{x}}{\bar{R}_b}, && y=\frac{\bar{y}}{N\bar{R}_b/\sqrt{\mathrm{Re}}}, && r_0=\frac{\bar{r}_0}{\bar{R}_b}, && u=\frac{\bar{u}}{\bar{u}^*},\\
&v=\frac{\bar{v}}{N\bar{u}^*/\sqrt{\mathrm{Re}}}, && \rho=\frac{\bar{\rho}}{\bar{\rho}_{sh}}, && T=\frac{\bar{T}}{\bar{T}_{st}}, && Cp=\frac{\bar{C}p}{\bar{C}p_{\mathrm{air}}},\\
&H=\frac{\bar{H}}{\bar{C}p_{\mathrm{air}}\bar{T}_{st}}, && \mu=\frac{\bar{\mu}}{\bar{\mu}_{sh}}, && \kappa=\frac{\bar{\kappa}}{\bar{\kappa}_{sh}}, && p=\frac{\bar{p}}{\bar{\rho}_{sh}\bar{u}^{*2}},
\end{aligned}\right\} \tag{2-8}$$

the fundamental equations can be reduced to

$$\frac{\partial(\rho u r_0)}{\partial x}+\frac{\partial(\rho v r_0)}{\partial y}=0, \tag{2-9}$$

$$\rho u\frac{\partial u}{\partial x}+\rho v\frac{\partial u}{\partial y}=-\frac{\partial p}{\partial x}+\frac{\partial}{\partial y}\left(\mu\frac{\partial u}{\partial y}\right), \tag{2-10}$$

$$\frac{N}{\sqrt{\mathrm{Re}}}\rho u^2=\frac{\partial p}{\partial y}, \tag{2-11}$$

$$\rho u\frac{\partial H}{\partial x}+\rho v\frac{\partial H}{\partial y}=\frac{\partial}{\partial y}\left[\frac{\mu}{Pr}\frac{\partial H}{\partial y}+\frac{W}{2}\mu\left(1-\frac{1}{Pr}\right)\frac{\partial u^2}{\partial y}\right], \tag{2-12}$$

where

$$H=CpT+\frac{W}{2}u^2, \tag{2-13}$$

and Re is Reynolds number defined by free stream conditions and radius of body curvature. Constants N and W are given in the symbol list.

As to the boundary layer flow with a favorable pressure gradient, estimation of order of magnitude of the left hand side of Eq. (2-11) gives [*13*]

$$O(N/\sqrt{\mathrm{Re}})\sim O(\bar{\delta}_j/\bar{R}_b),$$
$$\rho\sim O(1),\quad u\sim O(\bar{x}/\bar{R}_b),\quad \frac{\partial p}{\partial y}\sim O(\bar{\delta}_j/\bar{R}_b)$$

and $\bar{\delta}_j/\bar{R}_b$ can be neglected from the assumption. Therefore,

$$\frac{\partial p}{\partial y}=0,\qquad -\frac{\partial p}{\partial x}=\rho_e u_e\frac{du_e}{dx} \tag{2-14}$$

Since the free stream is hypersonic and the objective is a blunt nosed body of revolution, a constant density solution can be applied for the external flow. Thus,

$$\bar{u}_e=\bar{u}_\infty\sqrt{\frac{8\varepsilon}{3}}\frac{1}{1+\lambda}\sin x, \tag{2-15}$$

where ε and λ are density ratio of normal shock wave and non-dimensional shock stand-off distance, respectively, which are written as

$$\varepsilon=\frac{(\gamma-1)M_\infty^2+2}{(\gamma+1)M_\infty^2},\qquad \lambda=\frac{\varepsilon}{1+\sqrt{\frac{8\varepsilon}{3}-\varepsilon}} \tag{2-16}$$

If the reference value for normalization of velocity is chosen as

$$\bar{u}^*=\bar{u}_\infty\sqrt{\frac{8\varepsilon}{3}}\frac{1}{1+\lambda}, \tag{2-17}$$

velocity component at the outer edge of boundary layer is written as

$$u_e=\sin x. \tag{2-18}$$

Moreover, non-dimensional total enthalpy H_e is approximately unity. Therefore, from Eq. (2–13),

$$T_e=\frac{1-\frac{1}{2}Wu_e^2}{Cp_e}, \tag{2–19}$$

Viscosity can be written as

$$\bar{\mu}=266.93\times10^{-7}\frac{(M\bar{T})^{1/2}}{\bar{\sigma}^2\Omega^{(2)}} \quad (\mathrm{gr\cdot cm^{-1}\cdot sec^{-1}}) \tag{2–20}$$

according to Chapman-Enskog theory, where $\bar{\sigma}$ is collision diameter (Å) and $\Omega^{(2)}$ is non-dimensional collision integral which is obtained by the use of Lennard Jones (6, 12) potential in the temperature range under 1000°K. Consequently, relation between μ_e and T_e is

$$\mu_e=T_e^{1/2}. \tag{2–21}$$

At the outer edge of boundary layer, $\bar{C}p_e=\bar{C}p_{\mathrm{air}}$, so that

$$Cp_e=\bar{C}p_e/\bar{C}p_{\mathrm{air}}=1. \tag{2–22}$$

The assumption of constant density in the shock layer and the body geometry gives relations

$$\rho_e=1, \qquad r_0=\sin x. \tag{2–23}$$

Furthermore, Eqs. (2-13) and (2-19) reduce the temperature in the boundary layer to

$$\frac{T}{T_e}=\frac{H-(1/2)Wu^2}{(1-(1/2)Wu_e^2)Cp}. \tag{2–24}$$

Since the boundary layer gas is assumed perfect, the equation of state is also written at the outer edge in a similar way, therefore, the relation between density and temperature is

$$\frac{\rho_e}{\rho}=\frac{T}{T_e}. \tag{2–25}$$

The contribution of energy due to a vibrational or a rotational mode to the specific heat should be taken into account in the case of polyatomic gases, so that, the polynomial expression of specific heat such as

$$\bar{C}p=\bar{B}_1+\bar{B}_2\bar{T}+\bar{B}_3\bar{T}^2 \quad (\mathrm{cal\cdot gr^{-1}\cdot {}^\circ K^{-1}}) \tag{2–26}$$

should be written for air.

3. Transformation of Fundamental Equations

The fundamental equations, Eqs. (2-9) to (2-12), are the partial differential equations in the (x, y) coordinates system, and they can be transformed by introducing Lees-Dorodnitsyn transformation defined as

$$s=\int_0^x \rho_e\mu_e u_e r_0^2 dx, \qquad \eta=\frac{\rho_e u_e r_0}{\sqrt{2s}}\int_0^y \frac{\rho}{\rho_e}dy. \tag{3-1}$$

Stream function Ψ is defined as

$$\frac{\partial\Psi}{\partial x}=-\rho v r_0, \qquad \frac{\partial\Psi}{\partial y}=\rho u r_0. \tag{3-2}$$

and is further assumed to have a form

$$\Psi=\sqrt{2s}\,f(s,\eta). \tag{3-3}$$

Therefore, from Eqs. (3–1) and (3–3)

$$\frac{u}{u_e}=f'. \tag{3-4}$$

Enthalpy function is also defined as

$$\frac{H}{H_e}=g. \tag{3-5}$$

Transformed fundamental equations obtained from the above relations may be written as follows;

$$(Cf'')'+\beta\left(\frac{\rho_e}{\rho}-f'^2\right)+ff''=R_1, \tag{3-6}$$

$$\left(\frac{C}{Pr}g'\right)'+fg'+Wu_e^2\left[C\left(1-\frac{1}{Pr}\right)f'f''\right]'=R_2, \tag{3-7}$$

where $(\,)'$ represents the differentiation with respect to η, and

$$\beta=\frac{2s}{u_e}\frac{du_e}{ds}, \tag{3-8}$$

$$\left.\begin{aligned} R_1&=2s\left(f'\frac{\partial f'}{\partial s}-f''\frac{\partial f}{\partial s}\right),\\ R_2&=2s\left(f'\frac{\partial g}{\partial s}-g'\frac{\partial f}{\partial s}\right). \end{aligned}\right\} \tag{3-9}$$

Eq. (3-9) contains the derivatives of s-direction. The present problem is to obtain the non-similar solutions involving such non-similar terms as shown in Eq. (3-9).

The transformed coordinate s is related to x through Eq. (3-1), which, by the use

of Eqs. (2-18), (2-21) and (2-23), is reduced to

$$\begin{aligned} s&=\int_0^x\left(1-\frac{1}{2}W\sin^2 x\right)^{1/2}\sin^3 x\,dx \\ &=\left(\sqrt{\frac{2}{W}}\right)^3(I_1-I_2)\equiv s(x) \end{aligned} \tag{3-10}$$

where

$$\left.\begin{aligned} I_1&=\frac{1}{8}\left[2\xi_1\left\{\xi_1^2+\left(1-\frac{W}{2}\right)\right\}^{3/2}-\left(1-\frac{W}{2}\right)\xi_1\left\{\xi_1^3+\left(1-\frac{W}{2}\right)\right\}^{1/2}\right. \\ &\quad\left.-\left(1-\frac{W}{2}\right)^2\log\left|\xi_1+\sqrt{\xi_1^2+\left(1-\frac{W}{2}\right)}\right|-\sqrt{\frac{W}{2}}\left(1+\frac{W}{2}\right)\right], \\ I_2&=\frac{W}{4}\left[\xi_1\left\{\xi_1^2+\left(1-\frac{W}{2}\right)\right\}^{1/2}+\left(1-\frac{W}{2}\right)\log\left|\xi_1+\sqrt{\xi_1^2+\left(1-\frac{W}{2}\right)}\right|\right. \\ &\quad\left.-\sqrt{\frac{W}{2}}-\left(1-\frac{W}{2}\right)\log\left|\sqrt{\frac{W}{2}}+1\right|\right], \\ \xi_1&=\sqrt{\frac{W}{2}}\cos x. \end{aligned}\right\} \tag{3-11}$$

Transport properties C and Pr are Chapman-Rubesin number and Prandtl number, respectively, and are functions of f' and g.

Chapman-Rubesin number:

$$C=\frac{\bar{\rho}\bar{\mu}}{\bar{\rho}_e\bar{\mu}_e}=\frac{T_e}{T}\left(\frac{T}{T_e}\right)^{1/2}=\left(\frac{1-(1/2)Wu_e^2}{g-(1/2)Wu_e^2f'^2}\right)^{1/2}. \tag{3-12}$$

Prandtl number:

$$Pr=\frac{\bar{C}p\bar{\mu}}{\bar{\kappa}}=Pr_{\text{air}}Cp\frac{\mu/\mu_e}{\kappa/\kappa_e}=Pr_{\text{air}}Cp, \tag{3-13}$$

where Pr_{air} is Prandtl number of air and is a function of temperature.

For the purpose of treating the boundary conditions at the outer edge of the boundary layer, it may be convenient to introduce new variables defined as

$$\phi=f-\eta, \qquad \psi=g-1. \tag{3-14}$$

This means that;

(1) derivatives of the new variables with respect to η are

$$\phi'=f'-1, \quad \phi''=f'', \quad \phi'''=f''', \quad \psi'=g', \quad \psi''=g'', \tag{3-15}$$

so that boundary conditions at $\eta\to\infty$ can be replaced by zero, and the two-point boundary value problem is easily applied.

(2) truncation error, which arises when the difference of ρ_e/ρ and f'^2 in the second term of Eq. (3-6) is taken, may be avoided.

By using Eqs. (3-14) and (3-15), the fundamental equations, Eqs. (3-6) to (3-9), can be rewritten as

$$(C\phi'')'+\beta\left[\frac{\rho_e}{\rho}-(\phi'+1)^2\right]+\phi''(\phi+\eta)=R_1, \tag{3-16}$$

$$\left(\frac{C}{Pr}\phi'\right)'+\phi'(\phi+\eta)+Wu_e^2\left[C\left(1-\frac{1}{Pr}\right)(\phi'+1)\phi''\right]'=R_2, \tag{3-17}$$

where

$$\begin{aligned} R_1&=2s\left[(\phi'+1)\frac{\partial(\phi'+1)}{\partial s}-\phi''\frac{\partial(\phi+\eta)}{\partial s}\right],\\ R_2&=2s\left[(\phi'+1)\frac{\partial(\phi+1)}{\partial s}-\phi'\frac{\partial(\phi+\eta)}{\partial s}\right]. \end{aligned} \tag{3-18}$$

4. Boundary Conditions

From the definition of stream function, Eq. (3-2), the value of stream function along the wall is given by

$$\Psi_w=-\int_0^x(\rho v r_0)_w dx. \tag{4-1}$$

In the present approach, a step-wise distribution of $(\rho v)_w$ is assumed as shown in Fig. 2. Singularities in the streamwise derivative of Ψ_w exist at the points $x=x_1$, x_2, x_3, so that Eq. (4–1) becomes an improper integral. By use of a relation

$$\Psi_w=\sqrt{2s}\,\phi_w, \tag{4-2}$$

the reduced stream function ϕ_w at the wall may be, therefore, summarized as follow;

$$\text{(I)}\quad 0\leq x\leq x_1;\qquad \phi_w=-\dot{m}_f(1-\cos x)/\sqrt{2s}, \tag{4-3}$$

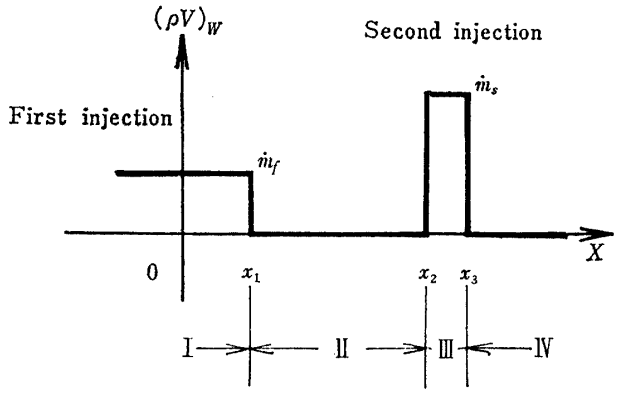

Fig. 2 Mass idjection distribution.

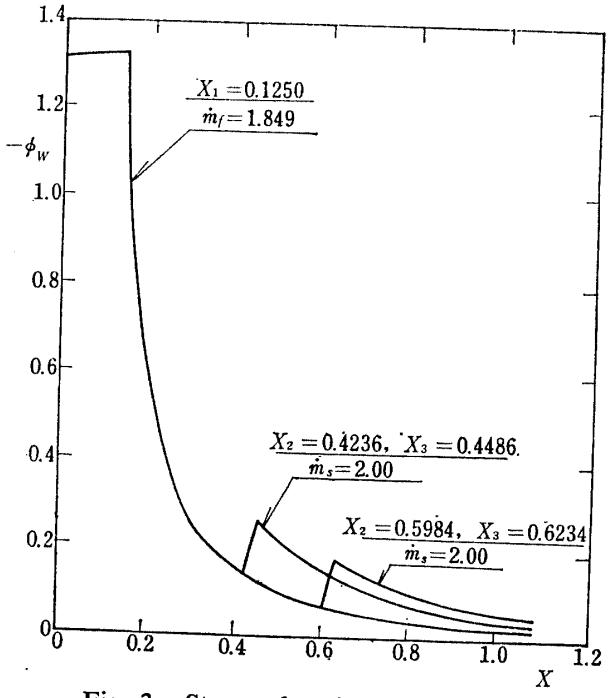

Fig. 3. Stream function distributions.

$$\text{(II)}\quad x_1<x<x_2;\qquad \phi_w=-\dot{m}_f(1-\cos x_1)/\sqrt{2s}, \tag{4–4}$$

$$\text{(III)}\quad x_2\leq x\leq x_3;\qquad \phi_w=-[\dot{m}_f(1-\cos x_3)+\dot{m}_s(\cos x_2-\cos x)]/\sqrt{2s}, \tag{4–5}$$

$$\text{(IV)}\quad x_3<x;\qquad \phi_w=-[\dot{m}_f(1-\cos x_1)+\dot{m}_s(\cos x_2-\cos x_3)]/\sqrt{2s}, \tag{4–6}$$

where the relation, $r_0=\sin x$ has been employed. Several examples concerning the distribution of ϕ_w are shown in Fig. 3. Non-dimensional injection parameters are defined by the equations

$$\dot{m}_f=\frac{\bar{\dot{m}}_f}{N\bar{\rho}_{sh}\bar{u}^*/\sqrt{\mathrm{Re}}},\qquad \dot{m}_s=\frac{\bar{\dot{m}}_s}{N\bar{\rho}_{sh}\bar{u}^*/\sqrt{\mathrm{Re}}}. \tag{4–7}$$

On the impermeable wall such as regions (II) and (IV) in Fig. 2, the stream function has the values equal to those of the points $x=x_1$ and x_3, respectively. Non-constant value of ϕ_w on the impermeable walls is clearly due to the transformation defined by Eq. (4–2) and, therefore, it should be remarked that ϕ does not correspond to the normal velocity component v directly.

Three kinds of wall conditions are considered in the present approach.

(1) an isothermal wall

The constant surface temperature $\bar{T}_w$ is given and $\bar{T}'_w$ which is the temperature gradient at the wall, is to be determined. The boundary conditions on the wall are;

$$\left.\begin{aligned}&\bar{u}=0\ \text{(non-slip)},\\ &\bar{H}=\bar{H}_w=\bar{C}p_w\bar{T}_w,\\ &\bar{v}=\bar{v}_w.\end{aligned}\right\}\quad\longrightarrow\quad\left\{\begin{aligned}&\phi'_w=-1,\\ &\phi_w=Cp_wT_w,\\ &\phi_w=\text{specified}.\end{aligned}\right\} \tag{4–8}$$

(2) an adiabatic wall

$\bar{T}'_w=0$ is given and the surface temperature $\bar{T}_w$ is determined. The boundary conditions on the wall are;

$$\left.\begin{aligned}\bar{u}&=0,\\ (\partial\bar{T}/\partial\bar{y})_w&=0,\\ \bar{v}&=\bar{v}_w.\end{aligned}\right\}\longrightarrow\left\{\begin{aligned}\phi'_w&=-1,\\ \phi'_w&=0,\\ \phi_w&=\text{specified.}\end{aligned}\right\}\tag{4-9}$$

(3) a coupled wall—wall is locally isothermal and locally adiabatic—

The third wall condition may be a good representation for the practical cases wherein the mass injection is utilysed to keep the adibatic wall temperature in steady flight at a tolerable level. The injection regions (I) and (III) are assumed to consist of the porous materials of which temperature is $\bar{T}_j$ (isothermal) and the regions (II) and (IV) are the adiabatic walls. The above boundary conditions on the wall are recapitulated as follows;

region	$(\rho v)_w$	wall condition	mathematical condition at $\eta=0$
(I) $0\leq x\leq x_1$	$\dot{m}_f$	porous wall ⟨isothermal⟩	$\phi'_w=-1$, $\phi_w=Cp_{jf}T_{jf}-1$, $\phi_w=$Eq. (4-3).
(II) $x_1<x<x_2$	0	impermeable wall ⟨adibatic⟩	$\phi'_w=-1$, $\phi'_w=0$, $\phi_w=$Eq. (4-4).
(III) $x_2\leq x\leq x_3$	$\dot{m}_s$	porous wall or slit ⟨isothermal⟩	$\phi'_w=-1$, $\phi_w=Cp_{js}T_{js}-1$, $\phi_w=$Eq. (4-5).
(IV) $x_3<x$	0	impermeable wall ⟨adiabatic⟩	$\phi'_w=-1$, $\phi'_w=0$, $\phi_w=$Eq. (4-6).

At the outer edge of the boundary layer, $\bar{u}=\bar{u}_e$, $\bar{H}=\bar{H}_e$, consequently,

$$\eta\rightarrow\infty\,;\quad \phi'=0,\quad \phi=0.\tag{4-10}$$

Here, it will be necessary to check whether the boundary layer approximation is valid for the local injection under consideration. In the boundary layer approximation it has been assumed that

$$\bar{v}\ll\bar{u},\qquad v_w<v_e.\tag{4-11}$$

In the present approach, validity of these conditions solely depends upon the magnitude of coolant mass flow rate and width of the injection slits. Because of this circumstance, the coolant mass flow rate $(\rho v)_w$ and the width of the injection slit $\bar{d}$ used in the numerical calculation are so chosen as to satisfy the conditions

$$\frac{(\rho v)_w}{(\rho v)_e}\sim O(10^{-2}),\qquad \bar{d}<\bar{\delta}_i\tag{4-12}$$

respectively, where $\bar{\delta}_j$ indicates thickness of oncoming boundary layer just upstream of the injection slit.

5. Method of Solution

5.1. *Outline of the H-W Method*

The H-W method developed by Hartree and Womersley [*19*] involves the procedure that the streamwise derivative is replaced by the corresponding difference to reduce the parabolic partial differential quations to the ordinary ones. The basic scheme of this method is diagramed in Fig. 4, and a solution $(S_n)k$ at the n-station is found out by integration in η-direction on the strip $s=s_n$, if the solutions have been found at all previous stations up to and including s_{n-1}.

It is based on the reason why downstream influences can not be felt upstream in equations of parabolic type.

The characteristics of the H-W method in the treatment of numerical analysis are;
(1) the difference method is implicit and always stable, so that the stability conditions are not necessary [*29*],
(2) both of s-direction difference and numerical integration in η-direction are independently made accurately,
(3) the step size of the difference form can be chosen arbitrarily.

Non-similar terms in the fundamental equations are the first-order derivatives in s-direction such as $\partial F/\partial s$, which are evaluated at the n-station as

$$\text{2-pt difference:}\quad \left(\frac{\partial F}{\partial s}\right)_n = \frac{F_n - F_{n-1}}{\Delta s_n} + \frac{\Delta s_n}{2}\frac{\partial^2 F(\xi)}{\partial s_n^2}, \tag{5-1-1}$$

$$\text{3-pt difference:}\quad \left(\frac{\partial F}{\partial s}\right)_n = (aF_n - bF_{n-1} + cF_{n-2}) + \frac{\Delta s_n(\Delta s + \Delta s_{n-1})}{6}\frac{\partial^3 F(\xi)}{\partial s_n^3}, \tag{5-1-2}$$

where the second terms of the right hand sides are the error terms accompanied

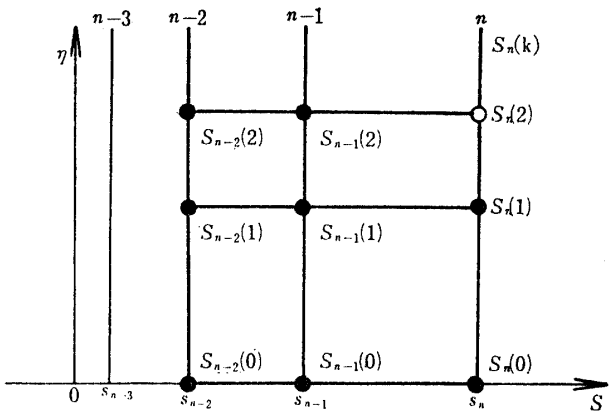

Fig. 4. Schematic diagram of the Hartree-Womersley method.

with the difference method and ξ is some value of s in the interval of (s_n-s_{n-1}) or (s_n-s_{n-2}). For an arbitrary interval, a, b and c can be determined as

$$a=\frac{1}{s_n-s_{n-1}}+\frac{1}{s_n-s_{n-2}}, \qquad b=\frac{s_n-s_{n-2}}{(s_n-s_{n-1})(s_{n-1}-s_{n-2})}, \qquad c=\frac{s_n-s_{n-1}}{(s_n-s_{n-2})(s_{n-1}-s_{n-2})}. \tag{5-1-3}$$

Reference [*21*] points out that the accuracy of the numerical calculation is not improved considerably even if 4-pt, 5-pt, etc. derivatives may be taken into consideration. Therefore, the difference is restricted up to 3-pt difference in the present approach.

5.2. *Solutions of One-Dimensional Heat Conduction Equation by the H-W Method*

In order to check the accuracy of the H-W method applied to the parabolic partial differential equations with discontinuous boundary conditions, one-dimensional heat conduction equation is considered. It is written as

$$\frac{\partial\theta}{\partial t}=\sigma^2\frac{\partial^2\theta}{\partial x^2}, \qquad \sigma=\text{const.} \tag{5-2-1}$$

where the initial and the boundary conditions are given as

$$\theta(x,0)=0, \tag{5-2-2}$$

$$\theta(0,t)=\text{given}, \qquad \theta(\infty,t)=0. \tag{5-2-3}$$

These equation and boundary conditions correspond to Eqs. (3-16) to (3-18) by replacing x by η, and t by s. The boundary conditions including singular points can be classified as followings.

At the singular point $(0, t_1)$,

⟨1⟩ functional value $F(t)$ is continuous, while its first-order derivative $\partial F/\partial t$ is discontinuous,

⟨2⟩ $F(t)$ is discontinuous, while $\partial F/\partial t$ is continuous,

⟨3⟩ both $F(t)$ and $\partial F/\partial t$ are discontinuous.

The difference forms, the adaptability of which is going to be checked, are specified as follows;

⟨I⟩ point form

the form in which the n-station exists just on $t=t_1$,

⟨II⟩ mean form

the form in which the singular point $t=t_1$ exists just on the middle point between $(n-1)$- and n-stations.

Furthermore, the difference methods mentioned in the previous section are summarized as follows;

⟨a⟩ 2-pt difference,

⟨b⟩ 3-pt difference,

⟨c⟩ common use of 3-pt and particular use of 2-pt differences.
The last difference method is that 2-pt difference is used only just aft of the singularity and the 3-pt difference is used for the remainder field.

Representative examples pertinent to each boundary condition can be tabulated in Table 1. Constants in this table are given as

$$\left.\begin{aligned} a&=\frac{\theta_0-\theta_1}{t_1(2t_2-t_1)}, \quad b=\theta_0-at_2^2=\theta_2, \quad c=\frac{\theta_1}{(t_1-t_2)^2}, \\ d&=0, \quad e=\frac{\theta_1-\theta_2}{(2t_2-t_1)^2}, \quad f=\frac{\theta_3}{(t_1-t_2)^2}. \end{aligned}\right\} \tag{5-2-4}$$

Since an analytical solution to Eq. (5-2-1) can be obtained exactly, the numeri-

TABLE 1. Classification of boundary conditions

classification	boundary condition	figure of boundary condition
< 1 >	$\theta(0,t)=\theta_1, \ (0\le t\le t_1)$ $=-\theta_1\frac{t-t_2}{t_2-t_1}, \ (t_1\le t\le t_2)$ $=0. \ (t_2\le t)$	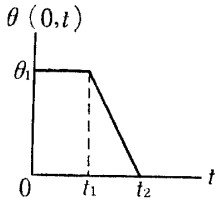
< 1 >	$\theta(0,t)=a(t-t_2)^2+b, \ (0\le t\le t_1)$ $=c(t-t_2)^2+d, \ (t_1\le t\le t_2)$ $=0. \ (t_2\le t)$	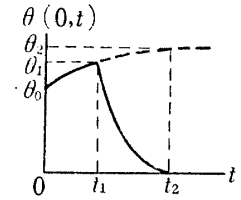
< 2 >	$\theta(0,t)=\theta_1 \ (0\le t\le t_1)$ $=0. \ (t_1\le t)$	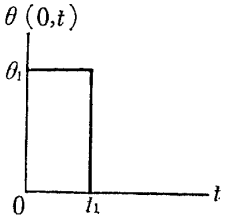
< 3 >	$\theta(0,t)=a(t-t_2)^2+b, \ (0\le t\le t_1)$ $=f(t-t_2)^2+e, \ (t_1\le t\le t_2)$ $=0. \ (t_2\le t)$	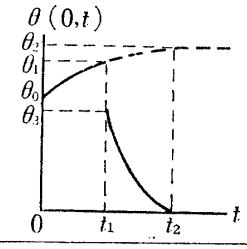

cal results calculated by use of the H-W method under the conditions

$$\theta_0=0.99,\ \theta_1=1.00,\ \theta_3=0.90,\ t_1=0.050,\ t_2=0.060,\ \sigma=6.325$$

were compared with the analytical ones at a point near aft of the singularity. In the numerical computations, integration in x-direction was reduced to two-point boundary value problem with edge conditions such as $\theta\to 0$ and $\partial\theta/\partial x\to 0$ at $x\to\infty$, starting with the initial value of $\partial\theta/\partial x$ estimated under the boundary conditions given in ⟨1⟩, ⟨2⟩ or ⟨3⟩. The numerical integrations in x-direction were carried out by Runge-Kutta-Gill method and the step size was 0.1. Convergency criterion which will be mentioned in Section 6.2 was taken as $E\leq 0.05$ corresponding approximately $\partial\theta/\partial x<0.15$ and $\theta<0.15$ at $x=x_{stop}$ and is not so strict. However this criterion seems to be reasonable because of the nature of asymptotic behavior of the solution.

Two problems arise in the numerical calculations. The first is the effect of variation of step size Δt on the solutions. Examination of the numerical results reveals that the difference method ⟨c⟩ may be compatible with the discontinuous

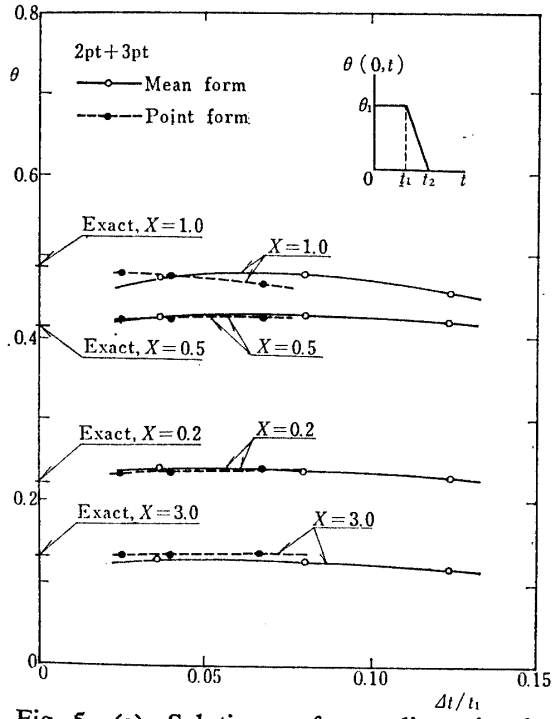

Fig. 5. (a) Solutions of one-dimensional heat conduction at $t=0.06$.
Boundary condition ⟨1⟩, $t_1=0.05$, $t_2=0.06$, $\sigma=6.325$, $\theta_1=1.00$.

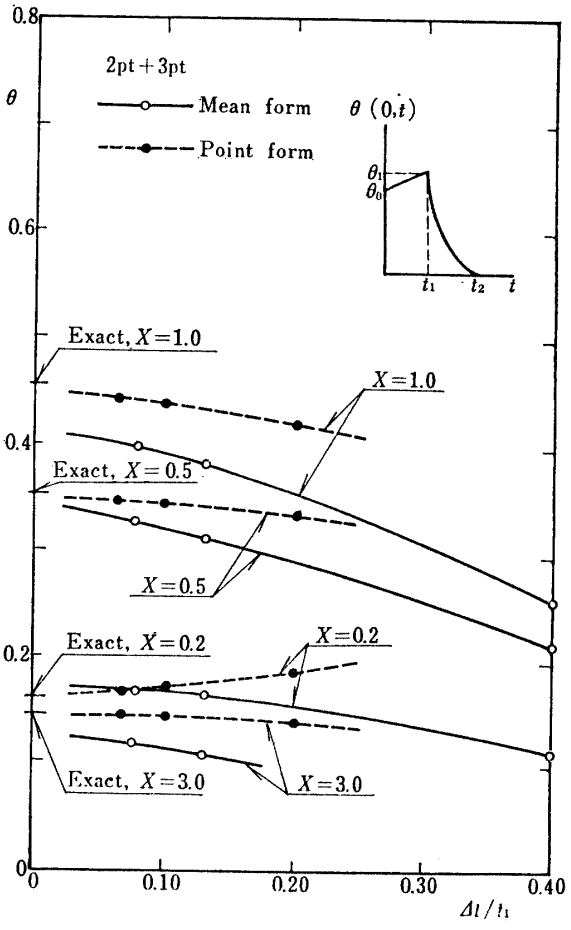

Fig. 5. (b) Continued.
Boundary condition ⟨1⟩, $t_1=0.05$, $t_2=0.06$, $\sigma=6.325$, $\theta_0=0.99$, $\theta_1=1.00$.

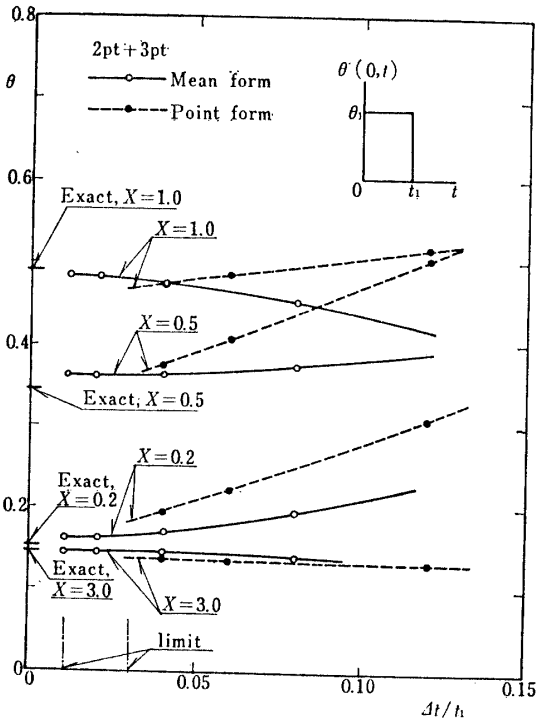

Fig. 5. (c) Continude.
Boundary condition ⟨2⟩, $t_1=0.05$. $t_2=0.06$, $\sigma=6.325$, $\theta_1=1.00$.

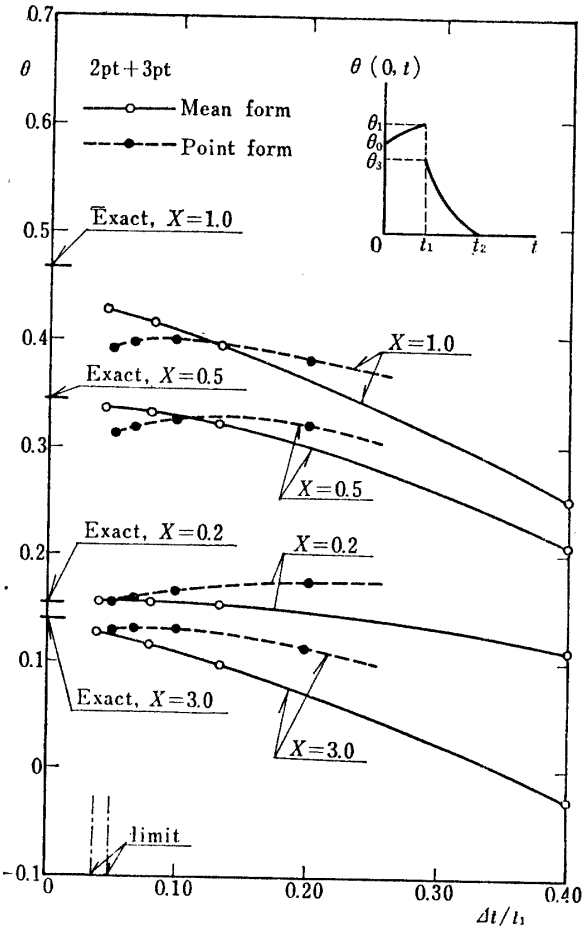

Fig, 5. Concluded.
Boundary condition ⟨3⟩, $t_1=0.05$, $t_2=0.06$, $\sigma=6.325$, $\theta_0=0.99$, $\theta_1=1.00$, $\theta_3=0.90$.

boundary conditions and the following remarks are obtained. For convenience' sake, let the boundary condition at $x=0$ be denoted by $F(t)$. If $F(t)$ is continuous while its derivative is discontinuous at $t=t_1$, then, it is natural that the solution should approach the exact one as Δt tends to zero. On the other hand, if $F(t)$ is discontinuous at $x=x_1$, $\lim_{\Delta t\to 0} \Delta F/\Delta t$ goes to infinity there and the solution diverges. In this case, limiting value of Δt for which the numerical solution can approach the exact one is restricted as is seen in Figs. 5(c) and (d).

The second is to find the proper difference form for each boundary condition. In Fig. 5 is further compared the mean form with the point form under the same criteria, and it is known that the point form is superior for the boundary condition of the type ⟨1⟩, and the mean form for ⟨2⟩ and ⟨3⟩, respectively.

However, as mentioned previously, the limits of the applicability of the mean form exist for the conditions ⟨2⟩ and ⟨3⟩, so that another form must be so taken as to make the limit free. This can be attained by the following procedure. Consider the condition ⟨2⟩ as an example. Since the boundary condition $\theta(0, t)$ is discontinuous at the point $(0, t_1)$ in this case and $\theta(0, t_1)$ has multi-values at this point, it

is necessary to obtain a single value θ_4 of $\theta(0, t_1)$ in order to make a difference at this point. Unfortunately, however, there seems to exist an infinite number of the choice of θ_4 in the range between zero and θ_1. Because of this circumstance, θ_4 was initially assumed and a solution was calculated at a point near aft of the singularity. The numerical solution thus obtained was next compared with the exact one and the error was estimated. This procedure was repeated, adjusting the value of θ_4 so as to reduce the error. Fig. 6 shows variation of the numerical solution with θ_4. It is seen in the figure that the value of θ_4 giving the accurate approximation near aft of the singularity approaches zero under the common use of 2-pt and 3-pt differences. This trend clearly indicates a fact that the value of θ_4 should be taken to be zero in making the difference starting from the singularity. This fact means that the difference should correspond to the right-derivative of the case ⟨2⟩.

The similar procedure was applied to the other cases of the boundary conditions and the following important results were obtained.

In the case ⟨1⟩, the point form gives the best approximation and the differences before and behind the singularity correspond automatically to the left- and right-

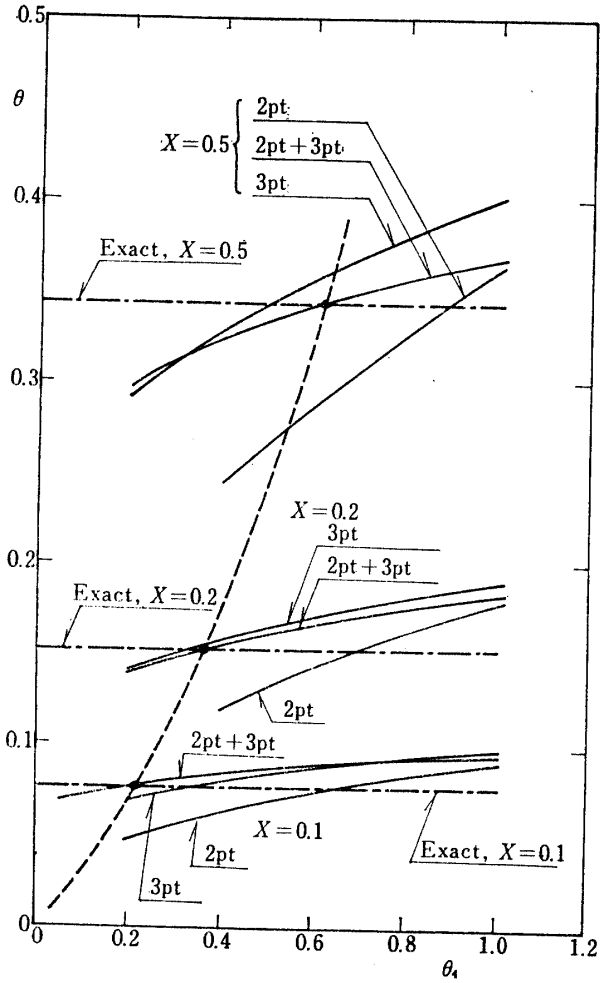

Fig. 6. Virtual value at singularity.
Boundary condition ⟨2⟩, $t=0.056$, $t_1=0.05$, $\sigma=6.325$.

derivatives of the function $F(t)$, respectively.

In the case ⟨2⟩, as mentioned above, the appropriate difference just ahead of the singularity should be made to be correspondent to the left-drivative of $F(t)$, while it should be made to be correspondent to the right-derivative just aft of the singularity. The same is true for the case ⟨3⟩.

These considerations lead to a statement that, with the difference method mentioned above, the H-W method is applicable to the parabolic partial differential equations with discontinuous boundary conditions.

5.3. *Application of the H-W Method to the Boundary Layer Equations*

The boundary condition, which has been set up in Chapter 4, is equivalent to the condition ⟨1⟩ classified in the previous section, in which the point form automatically satisfies the necessary requirements.

Non-similar terms in Eq. (3-18) are written by the use of Eqs. (5-1-1) to (5-1-3) as

$$\left.\begin{aligned} \text{2-pt;}\quad R_{1\,\text{two}} &= \frac{2s}{\Delta s}\{(\phi'+1)(\phi'-\phi'_{n-1})-\phi''(\phi-\phi_{n-1})\},\\ R_{2\,\text{two}} &= \frac{2s}{\Delta s}\{(\phi'+1)(\phi-\phi_{n-1})-\phi'(\phi-\phi_{n-1}),\} \end{aligned}\right\} \tag{5-3-1}$$

$$\left.\begin{aligned} \text{3-pt;}\quad R_{1\,\text{three}} &= 2s[(\phi'+1)\{a(\phi'+1)+b(\phi'_{n-1}+1)+c(\phi'_{n-2}+1)\}\\ &\qquad -\phi''\tilde{R}],\\ R_{2\,\text{three}} &= 2s[(\phi'+1)\{a(\phi+1)+b(\phi_{n-1}+1)+c(\phi_{n-2}+1)\}\\ &\qquad -\phi'\tilde{R}], \end{aligned}\right\} \tag{5-3-2}$$

where a, b and c are shown in Eq. (5–1–3) and

$$\tilde{R}=a(\phi+\eta)+b(\phi_{n-1}+\eta)+c(\phi_{n-2}+\eta). \tag{5-3-3}$$

6. Numerical Calculations and Discussions

6.1. *Properties and Models used in Calculations*

Both free stream and injectant consist of air and the numerical calculations were carried out under the conditions

$$\begin{aligned} &M_\infty=8,\quad \gamma=1.4,\quad \bar{T}_{st}=758^\circ\text{K},\quad \bar{p}_{st}=50\ \text{kg}\cdot\text{cm}^{-2},\\ &\bar{R}_b=2\ \text{cm},\quad \text{Re}=2.222\times10^5\ (\bar{R}_b=2\ \text{cm}),\\ &\bar{B}_1=0.2552\ \text{cal}\cdot\text{gr}^{-1}\cdot{}^\circ\text{K}^{-1},\quad \bar{B}_2=-9.25\times10^{-5}\ \text{cal}\cdot\text{gr}^{-1}\cdot{}^\circ\text{K}^{-2},\\ &\bar{B}_3=1.45\times10^{-7}\ \text{cal}\cdot\text{gr}^{-1}\cdot{}^\circ\text{K}^{-3},\qquad (300^\circ\text{K}<\bar{T}\leq550^\circ\text{K}),\\ &\bar{B}_1=0.2194\ \text{cal}\cdot\text{gr}^{-1}\cdot{}^\circ\text{K}^{-1},\quad \bar{B}_2=5.40\times10^{-5}\ \text{cal}\cdot\text{gr}^{-1}\cdot{}^\circ\text{K}^{-2},\\ &\bar{B}_3=0,\qquad\qquad\qquad\qquad (550^\circ\text{K}<\bar{T}),\\ &\text{Pr}=0.677+1.29\times10^{-4}\bar{T}_{st}T+1.26\times10^{-7}\bar{T}_{st}^2T^2, \end{aligned}$$

where properties of air are referred to [30] and $\bar{C}p_{\text{air}}=\bar{B}_1+\bar{B}_2\bar{T}+\bar{B}_3\bar{T}^2$.

Models have the first injection exit at the stagnation point and a ring slit at a downstream station. One model has the first injection only, and the other have the first injection with fixed geometry and the second one with different geometry.

6.2. *Two-Point Boundary Value Problem*

Since boundary conditions are given on the wall and the outer edge of the boundary layer, integration of the fundamental equations in η-direction is reduced to a two-point boundary value problem. Because of this, it is necessary to specify, at the wall, the same number of additional conditions as are required to be satisfied at the outer edge of the boundary layer in order to have the numerical integration start from the wall. There are two methods to approach this problem. The one is called "the initial value method" and another is "the quasilinearization method". Based on the viewpoint that the latter can not give the accurate solution, it is intended in this paper to present a refined method obtained by improving the initial value method extended by Nachtsheim and Swigert [*31*], which may be summarized as follows;

(1) assume the starting values,
(2) differentiate the original differential equations with respect to the assumed initial values, and obtain the complemental differential equations, which will be called "the perturbation equations",
(3) solve the original and the perturbation equations thus obtained simultaneously,
(4) judge convergence of the solutions by use of the criteria of the least square error between the imposed boundary conditions and the calculated values.

This method does not necessitate any limitation to the number of starting values, in principle. This characteristic is the most favorable advantage subjected to this method, while the other methods increase difficulty in solving the equations as the number of the initial values increases.

Let p and q be represented by the initial values to be found,

$$p=\phi_w'', \qquad q=\phi_w', \tag{6–2–1}$$

then the conditions at $\eta\to\infty$ can be written as

$$\left.\begin{aligned} \phi_e'(p,q)&=0, & \phi_e''(p,q)&=0,\\ \psi_e(p,q)&=0, & \psi_e'(p,q)&=0. \end{aligned}\right\} \tag{6–2–2}$$

Taking p_1 and p_2 as the first and the second approximations, respectively, the differences are written as

$$\Delta p=p_2-p_1, \qquad \Delta q=q_2-q_1. \tag{6–2–3}$$

For ϕ_e' and ψ_e, it is written that

$$\left.\begin{aligned} \Delta\phi_e'&=(\phi_e')_2-(\phi_e')_1, & \Delta\phi_e''&=(\phi_e'')_2-(\phi_e'')_1,\\ \Delta\psi_e&=(\psi_e)_2-(\psi_e)_1, & \Delta\psi_e'&=(\psi_e')_2-(\psi_e')_1, \end{aligned}\right\} \tag{6–2–4}$$

and by use of the abbreviations defined as $\partial/\partial p=(\ )_p, \partial/\partial q=(\ )_q$,

$$\left.\begin{aligned} \Delta\phi' &= \phi'_p\Delta p+\phi'_q\Delta q, & \Delta\phi'' &= \phi''_p\Delta p+\phi''_q\Delta q,\\ \Delta\psi &= \psi_p\Delta p+\psi_q\Delta q & \Delta\psi' &= \psi'_p\Delta p+\psi'_q\Delta q. \end{aligned}\right\} \tag{6-2-5}$$

Hence, the errors at $\eta=\eta_e$ are derived, by using Eqs. (6–2–4) and (6–2–5), as

$$\left.\begin{aligned} -\delta_1 &= \phi'+\phi'_p\Delta p+\phi'_q\Delta q, & -\delta_2 &= \phi''+\phi''_p\Delta p+\phi''_q\Delta q,\\ -\delta_3 &= \psi+\psi_p\Delta p+\psi_q\Delta q, & -\delta_4 &= \psi'+\psi'_p\Delta p+\psi'_q\Delta q, \end{aligned}\right\} \tag{6-2-6}$$

where the subscripts 1 and 2 are neglected for generality of the order of the approximation.

The square error is defined by

$$E=\sum_{k=1}^{4}\delta_k^2 \tag{6-2-7}$$

and the minimization of E requires the conditions

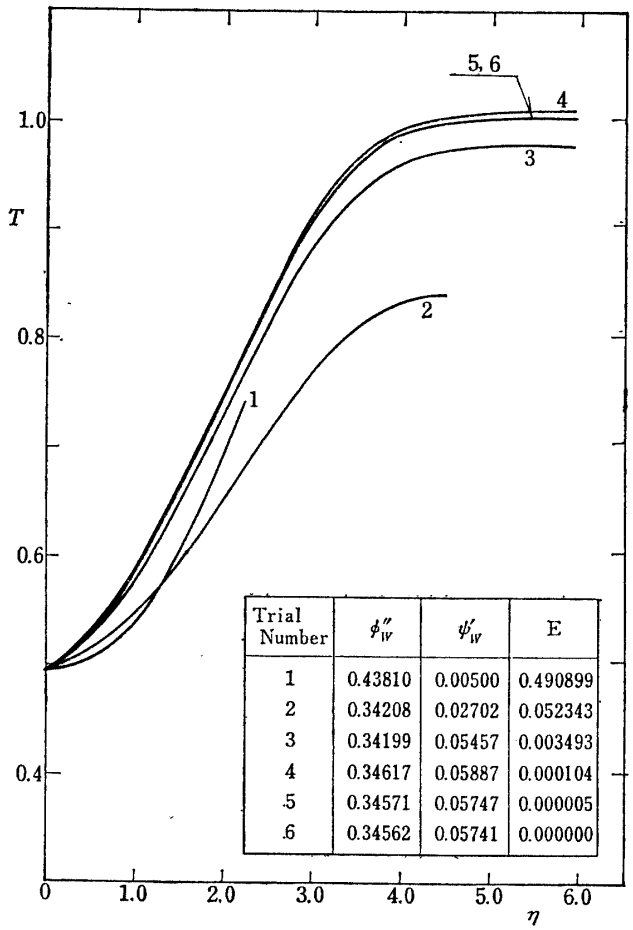

Trial Number	ϕ''_w	ψ'_w	E
1	0.43810	0.00500	0.490899
2	0.34208	0.02702	0.052343
3	0.34199	0.05457	0.003493
4	0.34617	0.05887	0.000104
5	0.34571	0.05747	0.000005
6	0.34562	0.05741	0.000000

Fig. 7. Convergence of solution of boundary layer equation. $x=0$, $\dot{m}_f=0.915$, $T_{jf}=0.492$.

$$\frac{\partial E}{\partial(\Delta p)}=0, \qquad \frac{\partial E}{\partial(\Delta q)}=0. \tag{6-2-8}$$

From Eq. (6-2-8),

$$\Delta p=-\frac{\begin{vmatrix} b_{12} & a_{12} \\ b_{22} & a_{22} \end{vmatrix}}{DEM}, \qquad \Delta q=-\frac{\begin{vmatrix} a_{11} & b_{12} \\ a_{21} & b_{22} \end{vmatrix}}{DEM}, \tag{6-2-9}$$

where

$$\left.\begin{aligned} a_{11}&=\phi_p'^2+\psi_p^2+\phi_p''^2+\psi_p'^2,\\ a_{12}&=\phi_p'\phi_q'+\psi_p\psi_q+\phi_p''\phi_q''+\psi_p'\psi_q',\\ a_{21}&=a_{12},\\ a_{22}&=\phi_q'^2+\psi_q^2+\phi_q''^2+\psi_q'^2,\\ b_{12}&=\phi'\phi_p'+\psi\psi_p+\phi''\phi_p''+\psi'\psi_p',\\ b_{22}&=\phi'\phi_q'+\psi\psi_q+\phi''\phi_q''+\psi'\psi_q',\\ DEM&=\begin{vmatrix} a_{11} & a_{12} \\ a_{21} & a_{22} \end{vmatrix}. \end{aligned}\right\} \tag{6-2-10}$$

The perturbation equations for ϕ and ψ with respect to p are written as

$$(C\phi'')_p'+\beta\left[\frac{\rho_e}{\rho}-(\phi'+1)^2\right]_p+\phi_p''(\phi+\eta)+\phi''\phi_p=R_{1p}, \tag{6-2-11}$$

$$\left(\frac{C}{Pr}\psi'\right)+\psi_p'(\phi+\eta)+\psi'\phi_p+Wu_e^2\left[C\left(1-\frac{1}{Pr}\right)(\phi'+1)\phi''\right]_p'=R_{2p}, \tag{6-2-12}$$

where the boundary conditions are given as

$$\left.\begin{aligned} \eta=0;\quad & \phi_p=\phi_p'=\psi_p=\psi_p'=0,\\ & \phi_p''=1. \end{aligned}\right\} \tag{6-2-13}$$

The perturbation equations for ϕ and ψ with respect to q have the similar forms to Eqs. (6-2-11) and (6-2-12) and the associated boundary conditions are given as

$$\left.\begin{aligned} \eta=0;\quad & \phi_q=\phi_q'=\phi_q''=\psi_q=0,\\ & \psi_q'=1. \end{aligned}\right\} \tag{6-2-14}$$

Since the solutions of these equations have essentially asymptotic behaviors at $\eta\to\infty$, the value of η_e becomes large as the iteration proceeds. Unfortunately, the solution is rather unstable at lower approximation and is sometimes divergent. In order to avoid these difficulties, the criteria

$$\phi'\leq 0.1,\ \phi''\geq 0.0,\ \psi\leq 0.2,\ \psi'\leq 0.2 \qquad \text{at } \eta=\eta_e \tag{6-2-15}$$

are set up, and if the solution misses any of them, the calculation is stopped. Then,

the next iteration starts with the assumed boundary conditions calculated by use of the data obtained in the last trial. The value of E in Eq. (6-2-7) represents the square error at each iteration and is a measure of the accuracy of the approximation. These calculations were carried out under the criterion $E \leq 10^{-5}$ in order to have accuracy of 10^{-3} for $\phi'_e, \phi''_e, \psi_e$ and ψ'_e.

Another problem is the uniqueness of solutions. It was proved numerically with the use of two sets of the initial values such as $\phi''_w=0.10000$, $T'_w=0.00100$ and $\phi''_w=0.4381$, $T'_w=0.00501$, where T'_w is used instead of ψ'_w for convenience. These data are shown in Table 2 together with the values of E. In the table, it is seen that, even if any set of the starting value of ϕ''_w and T'_w may be taken, it seems to converge to the unique one after six or seven trials, that is, ϕ''_w and T'_w approach to 0.1944 and 0.0095, respectively. Choice of the other set of the starting values gives the similar results, and it is desirable to choose suitable set so as to make the trial as few as possible.

TABLE 2. Convergency history of initial values ϕ''_w and T'_w in two-point boundary value problem. Isothermal wall case. $\dot{m}_f=0.915$, $x=0$.

Run 1				Run 2			
Trial number	ϕ''_w	T'_w	E	Trial number	ϕ''_w	T'_w	E
0	0.1000	0.00100	19.177	0	0.4381	0.00501	1.4961
1	0.1460	−0.01920	1.2175	1	0.2364	−0.06230	1.1006
2	0.2413	0.09972	1.4882	2	0.2091	−0.05870	0.7582
3	0.2149	0.03349	0.5882	3	0.1800	−0.00847	0.7281
4	0.1987	0.00823	0.1299	4	0.1983	0.01947	0.05793
5	0.1941	0.00889	0.00109	5	0.1963	0.01368	0.01053
6	0.1943	0.00955	0.000057	6	0.1945	0.00927	0.001144
				7	0.1944	0.00949	0.000077

6.3. *Adiabatic Wall Temperature Distribution*

The boundary conditions of the coupled wall defined in Chapter 4 are applied to obtain distribution of the adiabatic wall temperature. At the stagnation point, s-derivatives have finite values as $s \to 0$, hence $R_1 \to 0$, $R_2 \to 0$, so that the fundamental equations can be reduced to a set of the well known similar equations. In the adiabatic region, starting condition, $\psi'_w=0$, results in $\phi''_w=0$ which makes the solution invalid. Therefore, ψ'_w should be taken as small as possible. In many existing works it seems to be taken to be of order of 10^{-5}.

6.3.1. *Effect of Step Size Δx*

It is needless to say that the essential problem involved in the numerical solutions of this kind exists in accuracy of the solutions just behind the singularities. However, it must be noted that the physical feature of the singularity due to the second injection is similar to that due to the first one as shown in Fig. 3. Therefore, the

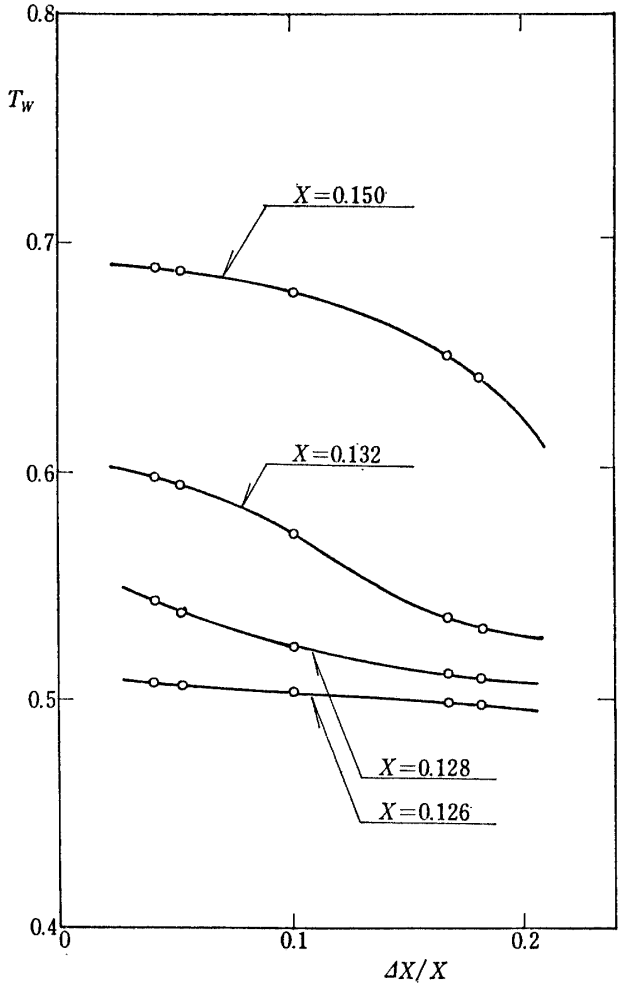

Fig. 8. Effect of of step size of on wall temperatnre. $\dot{m}_f=0.915$, $T_{fi}=0.492$.

discussion on the singularity is to be restricted to the former. In Fig. 8 is shown the effect of variation of step size Δx which is of importance for checking the accuracy of the solutions. Non-similar terms clearly depend upon the value of $\Delta x/x$. Computed solutions at $x=0.126$, 0.128, 0.132 and 0.150 (behind the singular point $x=x_1$ (=0.125)) give the following information; Δx should be taken small just behind the singularity, while at $x=0.150$ it is sufficient that $\Delta x/x$ is even 0.10. The favorable step size exists between 0.03 and 0.10 just aft of the singularity. Jaffe's attempt [*32*] also suggests that $\Delta x/x$ should be larger than 0.025. On the other hand, very large value of $x/\Delta x$ causes the instability in numerical integration in η-direction.

From the above results, the numerical calculations are carried out under the conditions as

$$0.1250 \leq x \leq 0.1503; \quad \Delta x=0.0063 \ (0.0418 \leq \Delta x/x \leq 0.0504),$$
$$0.1503 \leq x \leq 0.4033; \quad \Delta x=0.0253 \ (0.0627 \leq \Delta x/x \leq 0.1683),$$
$$0.4033 \leq x; \quad \Delta x=0.0500 \ (\Delta x/x \leq 0.1239).$$

Since the width of the second injection is 0.015 or 0.025 in each model, the value of $\Delta x/x$ becomes fairly small. Therefore, for the reason of stability and shortening of computational time, width of the slit is taken to be one difference step and computational point is put on the end of the slit.

6.3.2. *Downstream Effect of the First and the Second Injections*

Fig. 9(a) shows the computed results of the adiabatic wall temperature distribution with mass injection parameter 0.0, 0.915, 1.849 and 3.959. The wall temperatures on several points are shown in Fig. 9(b), where small mass injection rate is favorable for the adiabatic wall temperature. It is natural that the cooling effect decreases in downstream region.

Improvement of the cooling effectiveness due to the second injection is shown in Figs. 10(a) to (d) where the second injection rate $\dot{m}_s$ is taken up to 2.55 for the fixed $\dot{m}_c$ of 1.849. Numerical integrations were carried out in such a way that the initial value at each station is taken to be the converged one obtained at the previous station so as to speed up the computation. Step size in numerical integration by Runge-Kutta-Gill method was 0.1. Computational time for the first 28 stations existing between the stagnation point and the point $x=0.8$ was about 250 seconds

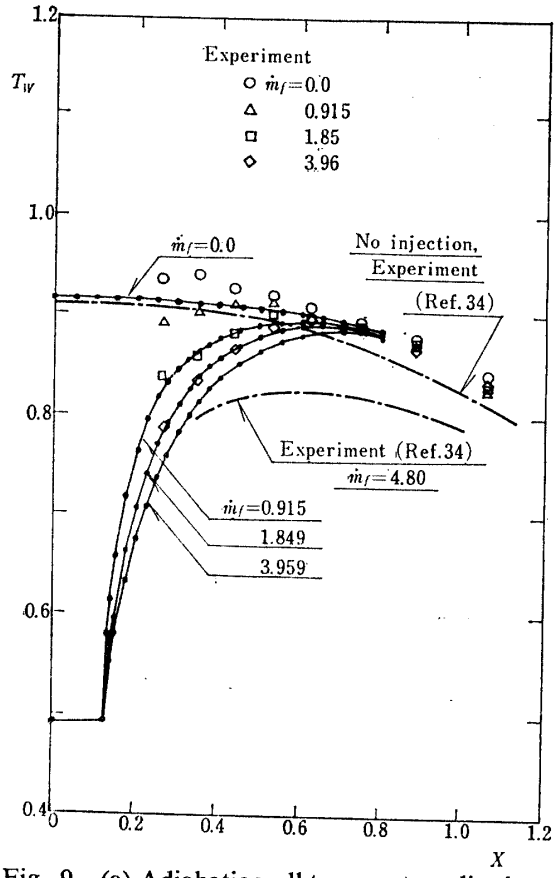

Fig. 9. (a) Adiabatic wall temperature distributions.
Central injection, $T_{jf}=0.492$, $x_1=0.1250$.

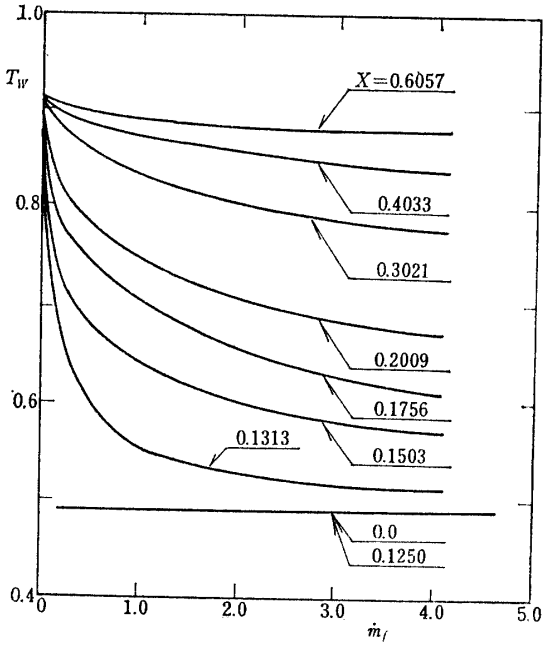

Fig. 9. (b) Variation of adiabatic wall temperature with first injection rate.
Central injection, $T_{jf}=0.492$, $x_1=0.1250$.

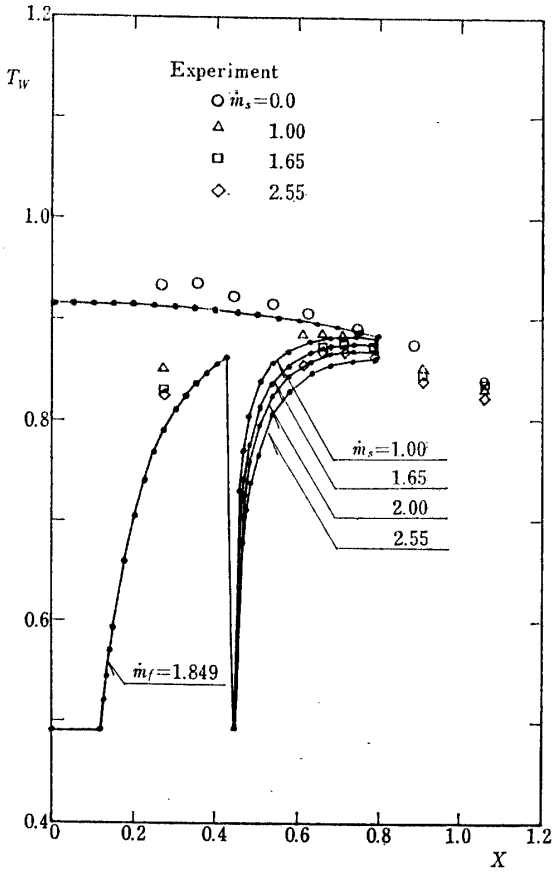

Fig. 10. Adiabatic wall temperature distributions with second injection.
(a) $x_1=0.1250$, $x_2=0.4286$, $x_3=0.4436$, $\dot{m}_f=1.849$, $T_{jf}=T_{js}=0.492$.

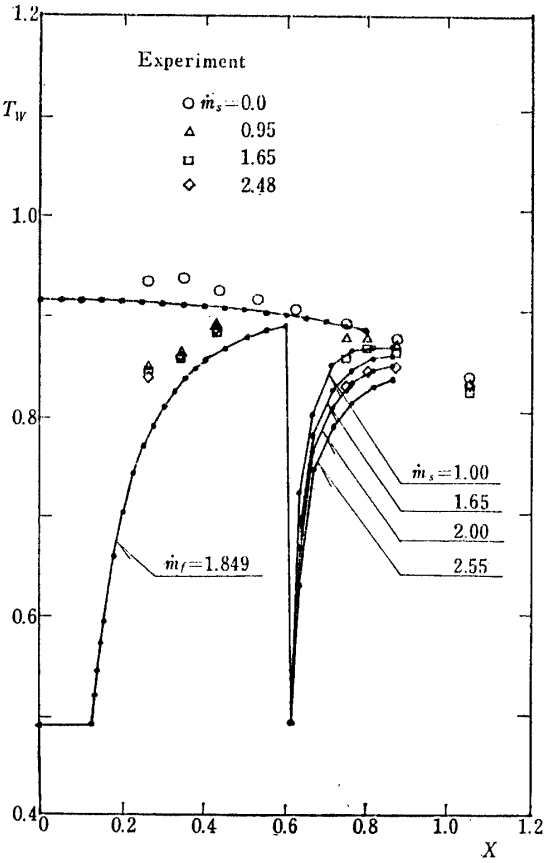

Fig. 10. Continued.
(b) $x_1=0.1250$, $x_2=0.6033$, $x_3=0.6183$, $\dot{m}_f=1.849$, $T_{jf}=T_{js}=0.492$.

by the use of HITAC 5020F at Data Processing Center in the Institute of Space and Aeronautical Science, University of Tokyo.

In Fig. 11 are presented temperature profiles in the boundary layer at several stations, in which η_e becomes smaller as x grows. However, this does not imply that the thickness of the boundary layer decreases with increase of x. Since the boundary layer thickness is given by the equation

$$\bar{\delta}_j=\frac{N\bar{R}_b}{\sqrt{\mathrm{Re}}}\frac{\sqrt{2s}}{\rho_e u_e r_0}\frac{1}{(1-(W/2)u_e^2)}\int_0^{\eta_e}\left[\phi+1-\frac{W}{2}u_e^2(\phi'+1)^2\right]d\eta, \qquad (6\text{–}3\text{–}2)$$

it still increases as x grows because of the existence of the term $\sqrt{2s}$ in the above equation.

6.3.3. *Estimation of Cooling Effectiveness with Several Mass Injection Parameters*

Let the mass injection parameters be taken as

(a) total injection mass flow; $\dot{W}$,

(b) position of injection slit; $\bar{\theta}$ (polar angle of mass injection station),

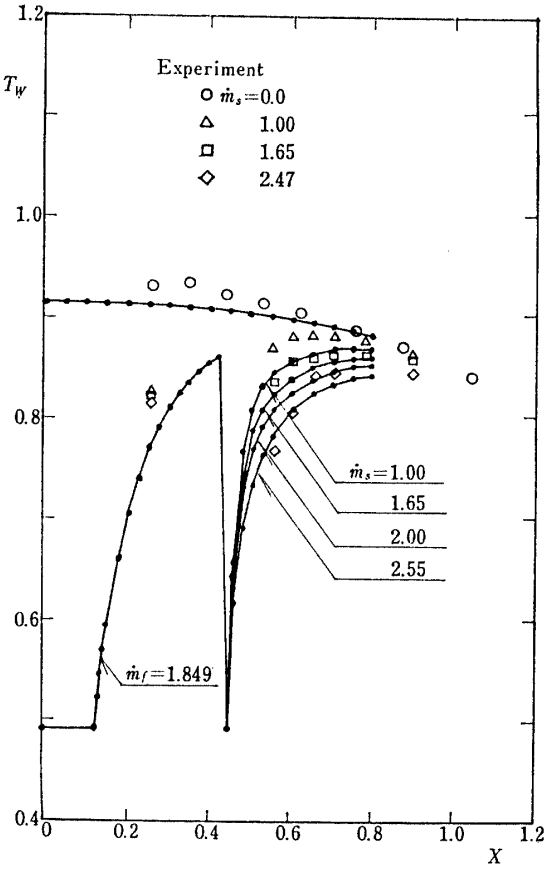

Fig. 10. Continued.
(c) $x_1=0.1250$, $x_2=0.4236$, $x_3=0.4486$, $\dot{m}_f=1.849$, $T_{jf}=T_{js}=0.492$.

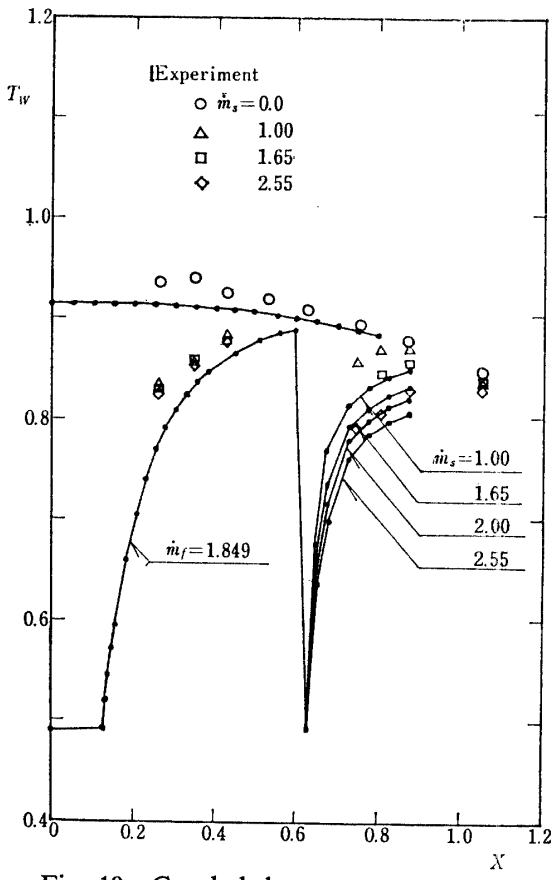

Fig. 10. Concluded.
(d) $x_1=0.1250$, $x_2=0.5984$, $x_3=0.6234$, $\dot{m}_f=1.849$, $T_{jf}=T_{fs}=0.492$.

(c) width of injection slit; $\bar{d}$.

Then, there seem to exist several criteria for representing the cooling effectiveness for an adiabatic wall such as

(1) maximum adiabatic wall temperature; $T_{w_{\max}}$,

(2) adiabatic wall temperature at a specified station; T_w,

(3) surface area kept below a specified wall temperature; Ar_c.

However, the first criterion seems to be less significant in actual results, so that the second and the third criteria are to be adopted in discussion on cooling effectiveness.

First, consider the second criterion. The total mass flow is written as

$$\dot{W}=\dot{m}A \tag{6-3-2}$$

where normalization quantities for $\dot{W}$ and A are $\bar{\dot{W}}^*=\dot{m}^*\bar{A}^*$ and $\bar{A}^*=2\pi\bar{R}_b^2$, respectively. It is seen in Fig. 9(b) that the small coolant mass flow rate (parameter (a)) is favorable both for the first and the second injections in the sense of cooling effectiveness.

The effect of the slit width (parameter (c)) may be discussed as follows. Fig. 12 presents the relation between the adiabatic wall temperature and the slit width for

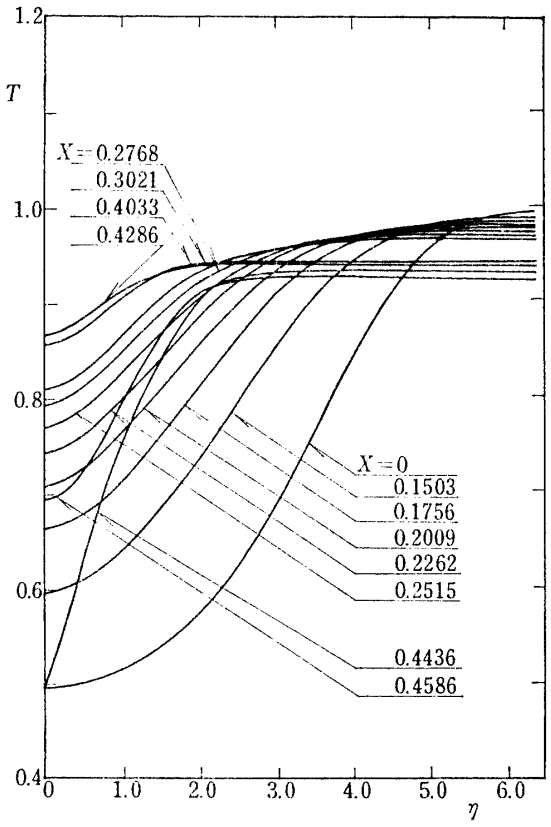

Fig. 11. Temperature profiles in boundary layer.
$x_1=0.1250$, $x_2=0.4286$, $x_3=0.4436$,
$\dot{m}_f=1.849$, $\dot{m}_s=2.00$,
$T_{jf}=T_{fs}=0.492$.

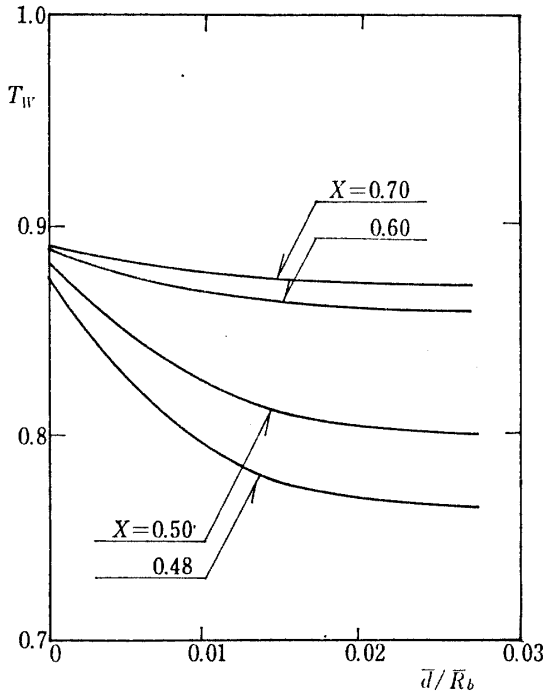

Fig. 12. Variation of adiabatic wall temperature with slit width of second injection. $\dot{W}=0.0249$.

the case of $\dot{W}=0.0249$. The figure clearly indicates that the effect of the slit width is small under the condition of the constant total mass flow. This leads to the useful conclusion from the engineering viewpoint that the slit width can be lessened without loss of cooling effectiveness.

Now, consider the third criterion. The nomenclature Ar_c means the surface area where the wall temperature is kept below some critical value T_{w_c}. It can be connected with the corresponding streamwise distance x_c as illustrated in Fig. 13.

Under the condition of the constant total mass flow ($\dot{W}=0.0208$), the adiabatic wall temperature distributions due to the various location of the second injection are obtained as in Fig. 14. Cooling effectiveness for an adiabatic wall is defined as

$$\Lambda_c=\frac{Ar_c}{\dot{W}} \qquad (6\text{–}3\text{–}3)$$

and the results are shown in Fig. 15 with the critical wall temperature $T_{w_c}=0.862$. In the figure it is seen that the second injection (parameter (b)) should be located at the point where the wall temperature T_w is as high as the critical wall temperature T_{w_c}, and that the effect of the slit width $\bar{d}/\bar{R}_b$ (parameter (c)) is also small.

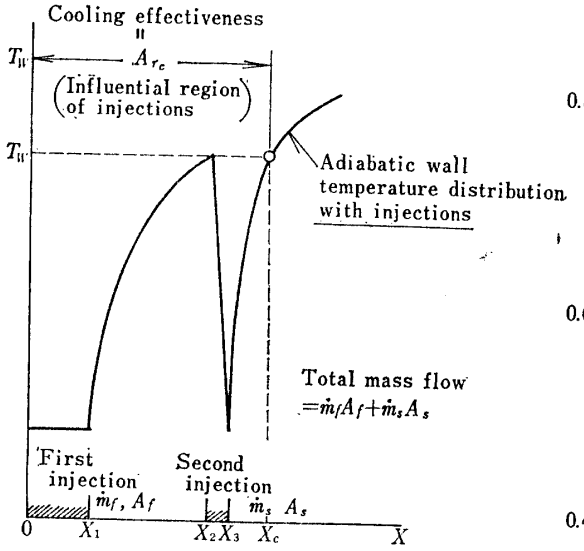

Fig. 13. Illustration indidating cooling effectiveness for adiabatic wall case.

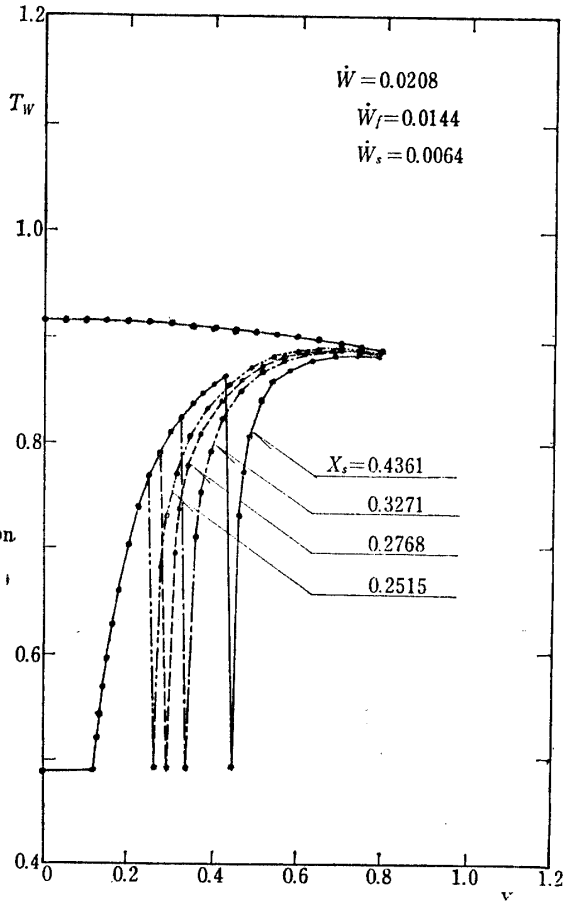

Fig. 14. Effect of position of second injection on adiabatic wall temperature distribution. $M_\infty=8$, $T_{jf}=T_{js}=0.492$, $\bar{d}/\bar{R}_b=0.015$.

In Fig. 16 is shown the adiabatic wall temperature distribution associated with the various mass flow of the first injection where the total mass flow is kept constant. The corresponding cooling effectiveness is shown in Fig. 17, where the optimum mass flow ratio is seen to exist at about $\dot{W}_s/\dot{W}=0.3$.

6.4. *Heat Transfer Distribution*

Heating rate is calculated under the assumption of an isothermal wall condition. It is defined as

$$-\dot{\bar{q}}_w=\left(\bar{\kappa}\frac{\partial\bar{T}}{\partial\bar{y}}\right)_w, \qquad (\mathrm{cal\cdot cm^{-2}\cdot sec^{-1}}) \qquad (6\text{–}4\text{–}1)$$

and is further reduced to

$$-\dot{q}_w=-\frac{\dot{\bar{q}}_w}{\dot{\bar{q}}^*}=\frac{\rho_w u_e r_0 \kappa_w}{\sqrt{2s}}T'_w, \qquad (6\text{–}4\text{–}2)$$

where

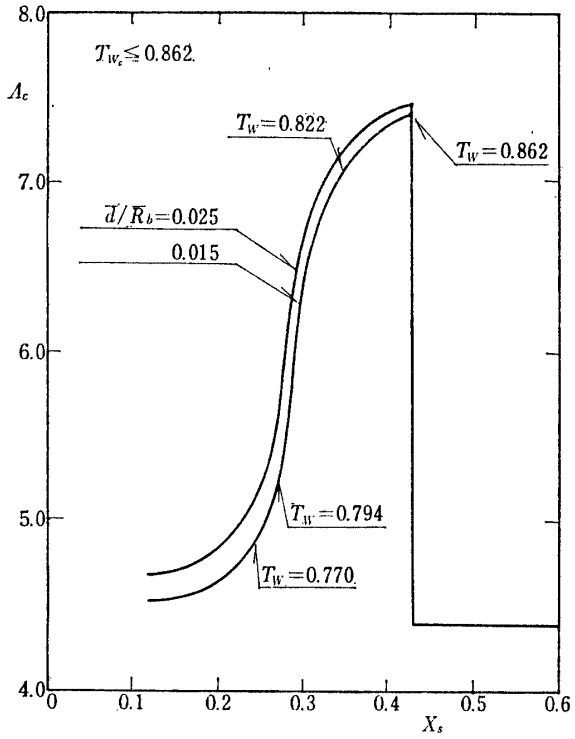

Fig. 15. Cooling effectiveness for adiabatic wall case: Effect of position of second injection with constant total mass flow.
$\dot{W}=0.0208$, $\dot{W}_f=0.0144$,
$\dot{W}_s=0.0064$, $T_{jf}=T_{js}=0.492$.

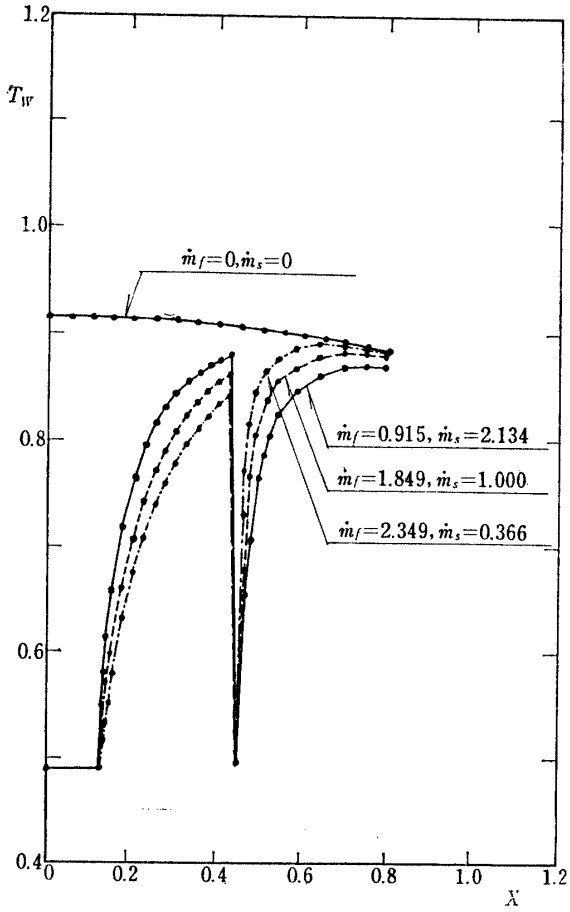

Fig. 16. Effect of mass flow of second injection on adiabatic wall temperature distribution. $M_\infty=8$, $x_s=0.4361$, $T_{jf}=T_{js}=0.492$, $\bar{d}/\bar{R}_b=0.015$.

$$\dot{\bar{q}}^*=\frac{\bar{\kappa}_{\text{air}}\bar{T}_{st}\sqrt{\overline{\text{Re}}}}{N\bar{R}_b}. \qquad (\text{cal}\cdot\text{cm}^{-2}\cdot\text{sec}^{-1}) \qquad (6\text{–}4\text{–}3)$$

6.4.1. Downstream Effects of the First and the Second Injection

Results of the numerical calculations with $T_w=0.492$ and $\dot{m}_f=0.0$, 0.915 and 1.849 are shown in Fig. 18 where the heat transfer rate increases rapidly behind the slit. Comparing Fig. 18 with Fig. 9(a), it is seen that the maximum local heating appears upstream of the position of the maximum adiabatic wall temperature for the same injection rate. This means that the influential region of the first injection is narrower for the heating rate rather than for the adiabatic wall temperature. For the second injection of four computational models the results of $\dot{m}_s=1.00$ and 2.00 are shown in Figs. 19(a) and (b). Present results obtained for no injection are also compared with the analytical ones proposed by Lees [*33*] in the same figure. It is seen that the error of the present calculation is about 8% at $x=0.8$ which can be considered to be allowable.

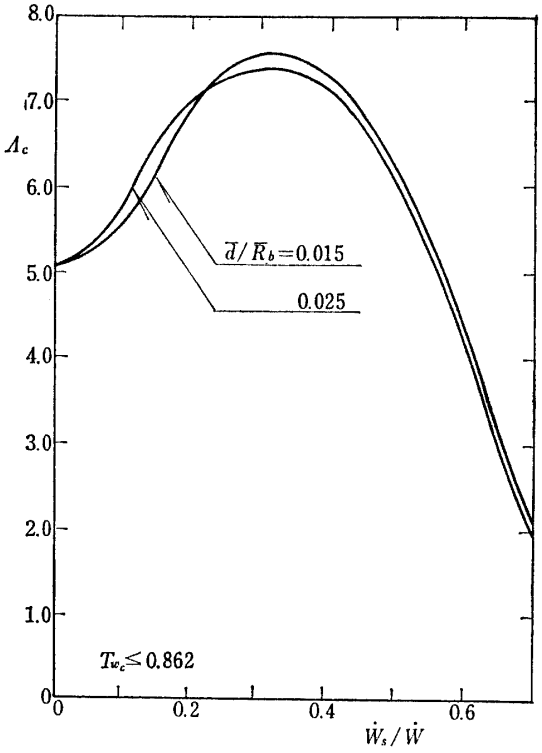

Fig. 17. Cooling effectiveness of adiabatic wall case: Effect of mass flow of second injection with constant total mass flow. $\dot{W}=0.0208$, $x_s=0.4361$, $T_{jf}=T_{js}=0.492$.

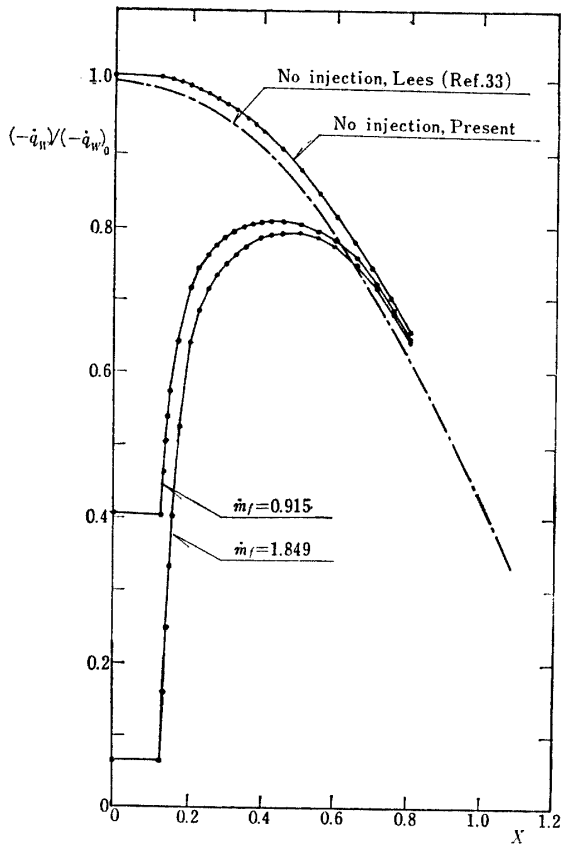

Fig. 18. Heat transfer rate distributions with first injection. Central injection.
$T_w=0.492$.

6.4.2. *Estimation of Cooling Effectiveness*

Integration of the heat transfer rate over the body surface is equal to overall heat input. Heat transferred per unit time onto the body surface within the region from the stagnation point to the point $x=x_q$ is given as

$$\bar{Q}=\int_0^{x_q}(-\dot{\bar{q}})d\bar{A}. \tag{6-4-4}$$

Let $\bar{Q}_{no}$ and $\bar{Q}_L$ be denoted by the heat inputs without injection and with local injection, respectively, then, $(\bar{Q}_{no}-\bar{Q}_L)$ is the heat shielded by the local injection. Therefore, if the cooling effectiveness is defined as

$$H_{c_L}=\frac{\bar{Q}_{no}-\bar{Q}_L}{(\bar{H}_e-\bar{H}_w)\int_0^{x_q}\dot{\bar{m}}d\bar{A}}, \tag{6-4-5}$$

then, it is proportional to the heat absorbed in the unit mass of coolant per unit time.

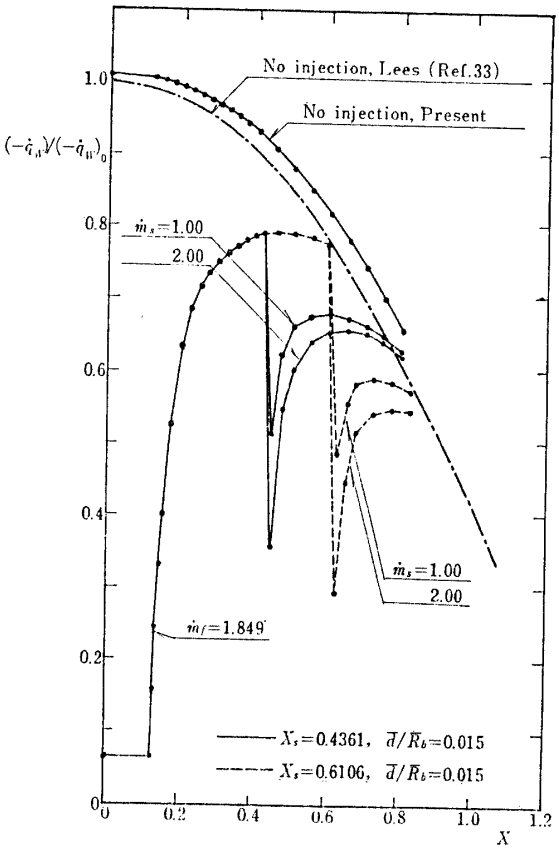

Fig. 19. Heat transfer rate distributions with second injection.
(a) $\bar{d}/\bar{R}_b=0.015, T_w=0.492$, $\dot{m}_f=1.849$.

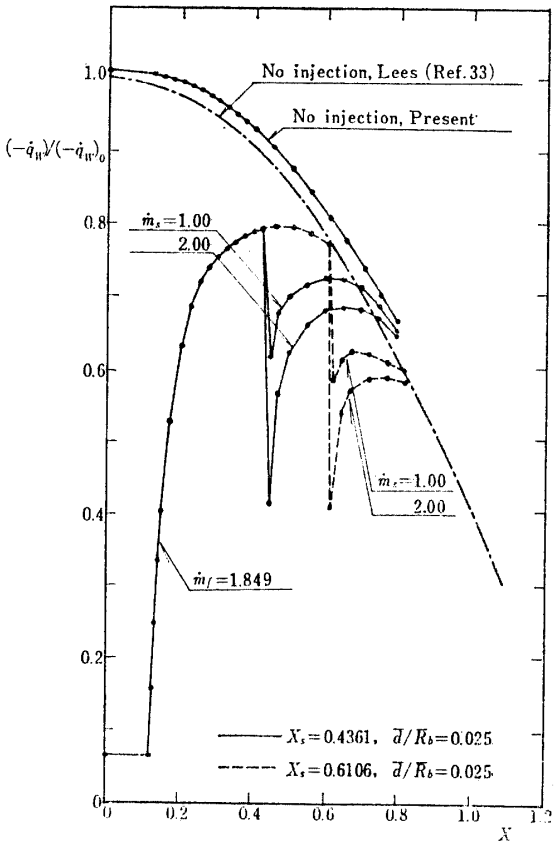

Fig. 19. Concluded.
(b) $\bar{d}/\bar{R}_b=0.025$, $T_w=0.492$, $\dot{m}_f=1.849$.

Fig. 20(a) shows the cooling effectiveness thus calculated. Non-dimensional distance x_q is taken as 0.8283.

As to the effect of the cooling parameter (a), the results show the similar trend to the coupled wall case. As to parameter (b), the results show that the position of the second injection $x_s=0.4361$ is superior to $x_s=0.6106$. The peak point of the heat transfer distribution without the second injection is located at about the point $x_p=0.45$, therefore, it is advantageous that the position of the slit should be situated at slightly ahead of x_p.

In Fig. 20(b) is shown the optimum width for the injection mass flow. The trend involving the optimum values arises from the following reason; the total mass flow $\dot{W}$ is represented by product of mass flow rate and the injection area, therefore, with $\dot{W}$ kept constant, the cooling effectiveness is determined by a coupling of increase of the downstream influential region due to increase of A with reduction of heat shielding due to decrease of $\dot{m}$, and vice versa.

6.5. *Comparison of Cooling Effectiveness with Transpiration Cooling*

In order to compare the effectiveness of the local injection cooling with that of the transpiration cooling, the equivalent transpiration cooling is defined as an uni-

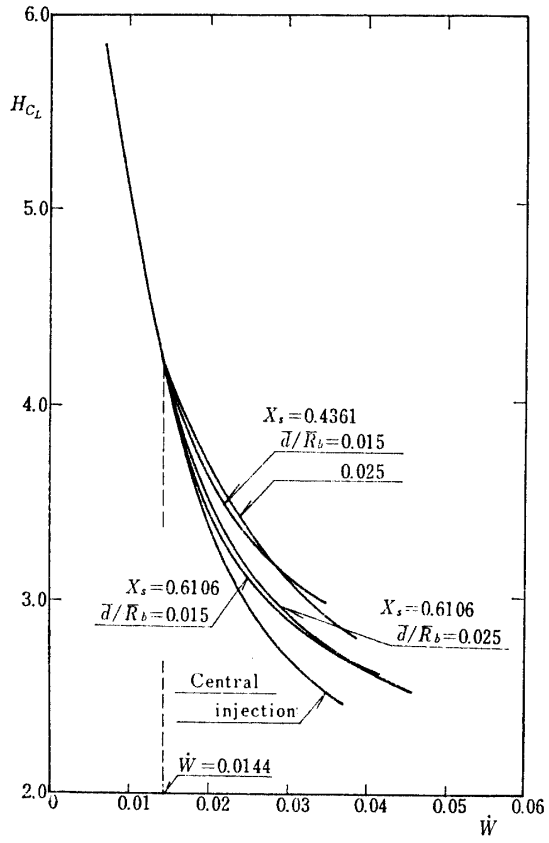

Fig. 20. Cooling effectiveness f or isothermal wall case.
(a) Effect of total mass flow, $T_w=0.492$.

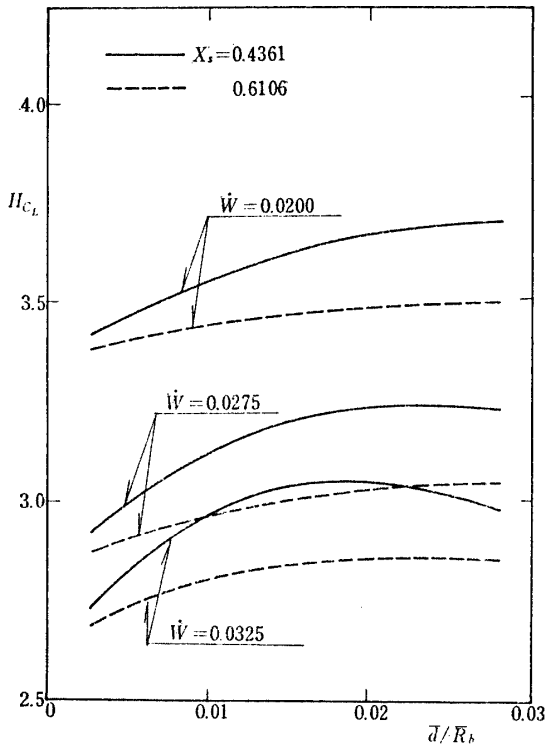

Fig. 20. Concluded.
(b) Eflect of width of injection exit, $T_w=0.492$.

form injection cooling over a finite range of the surface with the same total coolant mass flow as that of the associated local injection cooling, that is,

$$\dot{m}_T A_T=\dot{m}_f A_f+\dot{m}_s A_s, \tag{6-5-1}$$

where A_T denotes the area of the equivalent transpiration cooling and $\dot{m}_T$ is the associated coolant mass flow rate. Therefore, it must be noted that, if the total coolant mass flow of the local injection is kept constant, the mass flow rate of the equivalent transpiration cooling is a function of the transpiration area under consideration.

With the definition, the effectiveness of the transpiration cooling defined up to the point $x=x_q$ is written as

$$H_{c_T}=\frac{\bar{Q}_{no}-\bar{Q}_T}{(\bar{H}_e-\bar{H}_w)\int_0^{x_q}\dot{\bar{m}}d\bar{A}}, \tag{6-5-2}$$

and by use of the corresponding effectiveness of the equivalent local injection cooling, it can be rewritten as

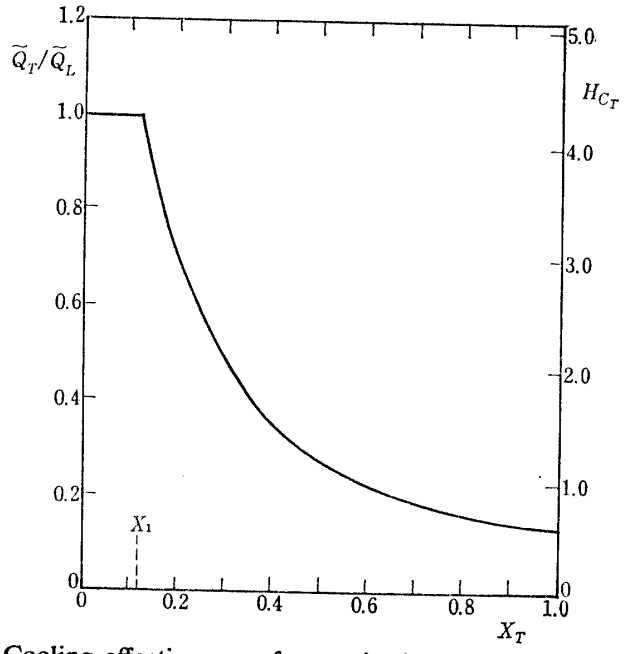

Fig. 21. Cooling effectiveness of transpiration cooling system equivalent to central injection model. $T_w=0.492$. $\dot{m}_f=1.849$.

$$H_{c_T}=\frac{\bar{Q}_{no}-\bar{Q}_L}{(\bar{H}_e-\bar{H}_w)\int_0^{x_q}\dot{m}d\bar{A}}\frac{\bar{Q}_{no}-\bar{Q}_T}{\bar{Q}_{no}-\bar{Q}_L}=H_{c_L}\frac{\bar{Q}_T}{\bar{Q}_L}, \qquad (6\text{–}5\text{–}3)$$

where $\bar{Q}_T/\bar{Q}_L$ represents a ratio of heat shielded by the transpiration cooling to that by the local injection cooling.

For the transpiration model equivalent to the central injection model, $\bar{Q}_T/\bar{Q}_L$ is shown in Fig. 21, where

$$x_T=x_1:\ \bar{Q}_T/\bar{Q}_L=1,$$
$$x_T>x_1:\ \bar{Q}_T/\bar{Q}_L<1.$$

Consequently, from Eq. (6-5-3), it is found that the local injection cooling is always more effective than the transpiration cooling without loss of generality. This is clearly due to the small heat transfer rate near the injection slit in the case of the local injection cooling. This, in turn, leads further to the remarkable statement that the concentrated injection at the stagnation point is the most effective.

7. Experiment

7.1. *Experimental Conditions and Models*

For the purpose of confirming the accuracy of the present approach measurement of the adiabatic wall temperature distribution over spherical models with local injection was carried out by use of a hypersonic wind tunnel under the following test conditions;

free stream Mach number $M_\infty = 8$,
total temperature $\bar{T}_{st} = 485 \pm 15°C$,
total pressure $\bar{p}_{st} = 50 \pm 0.5\ \mathrm{kg \cdot cm^{-2}}$,
free stream Reynolds number $\mathrm{Re} = 2.22 \times 10^5$ ($\bar{R}_b = 2$ cm).

Five hemispherical models made of FRP which are shown in Table 3 were used to specify the slit geometry. Wall temperature was measured by use of 0.64 mm$^\phi$ $C-A$ thermocouples which are mounted on the model surface together with 2 mm$^\phi \times 2$ mm copper calorimeters attached to the tips. Sizes of models and temperature sensors are shown in Fig. 22. Thermal properties of FRP are

heat conduction coefficient $\kappa = 6.4 \times 10^{-4}\ \mathrm{cal \cdot sec^{-1} \cdot cm^{-1} \cdot °K^{-1}}$,
specific heat $\bar{C}p = 0.23 \sim 0.25\ \mathrm{cal \cdot gr^{-1} \cdot °K^{-1}}$,

so that the adiabatic wall condition may be satisfied fairly well because coefficient of heat conduction of FRP is 0.003 times the steel value.

TABLE 3. Dimensions of models.

Model	x_1	x_2	x_3	$\bar{A}_f$	$\bar{A}_s$	$\bar{\theta}$	$\bar{d}$	$\bar{d}/\bar{R}_b$
dimension				(cm^2)	(cm^2)	(deg)	(mm)	
A	0.1250	—	—	0.1963	—	—	—	—
B	0.1250	0.4286	0.4436	0.1963	0.1608	25	0.3	0.015
C	0.1250	0.6033	0.6183	0.1963	0.2185	35	0.3	0.015
D	0.1250	0.4236	0.4486	0.1963	0.2650	25	0.5	0.025
E	0.1250	0.5984	0.6234	0.1963	0.3617	35	0.5	0.025

The first injection exit consists of porous plug made of 70 μ sintered metal, and ring slit is situated at the position of polar angle ($\bar{\theta}$) equal to 25° or 35° as the second injection exit. Coolant is injected independently out of them.

Mass flow rate was regulated by use of a float type flow meter. The temperature inside the porous plug seldom changes and is kept almost constant equal to the injectant value during the operation, because the coolant velocity is not so large. Surface temperature was measured at 8 stations (see Fig. 22). FRP material changed its color slightly during the 10~20 operations and the surface was slightly charred, but the roughness is not so serious as to induce boundary layer transition.

7.2. *Reduction of Experimental Results*

An experimental duration determined by the operation time of the wind tunnel is about 90 seconds, and during that time, the transient wall temperature was measured. Therefore, the equilibrium wall temperature was reduced in the following way. Non-equilibrium characteristics of the surface temperature are considered according to the transient heat flow from the boundary layer to the copper calorimeter, so that, by estimating the heat flow, a relation between transient temperature $\bar{T}_w(\bar{t})$ and the equilibrium temperature $\bar{T}_{eq}$ was assumed to have a form

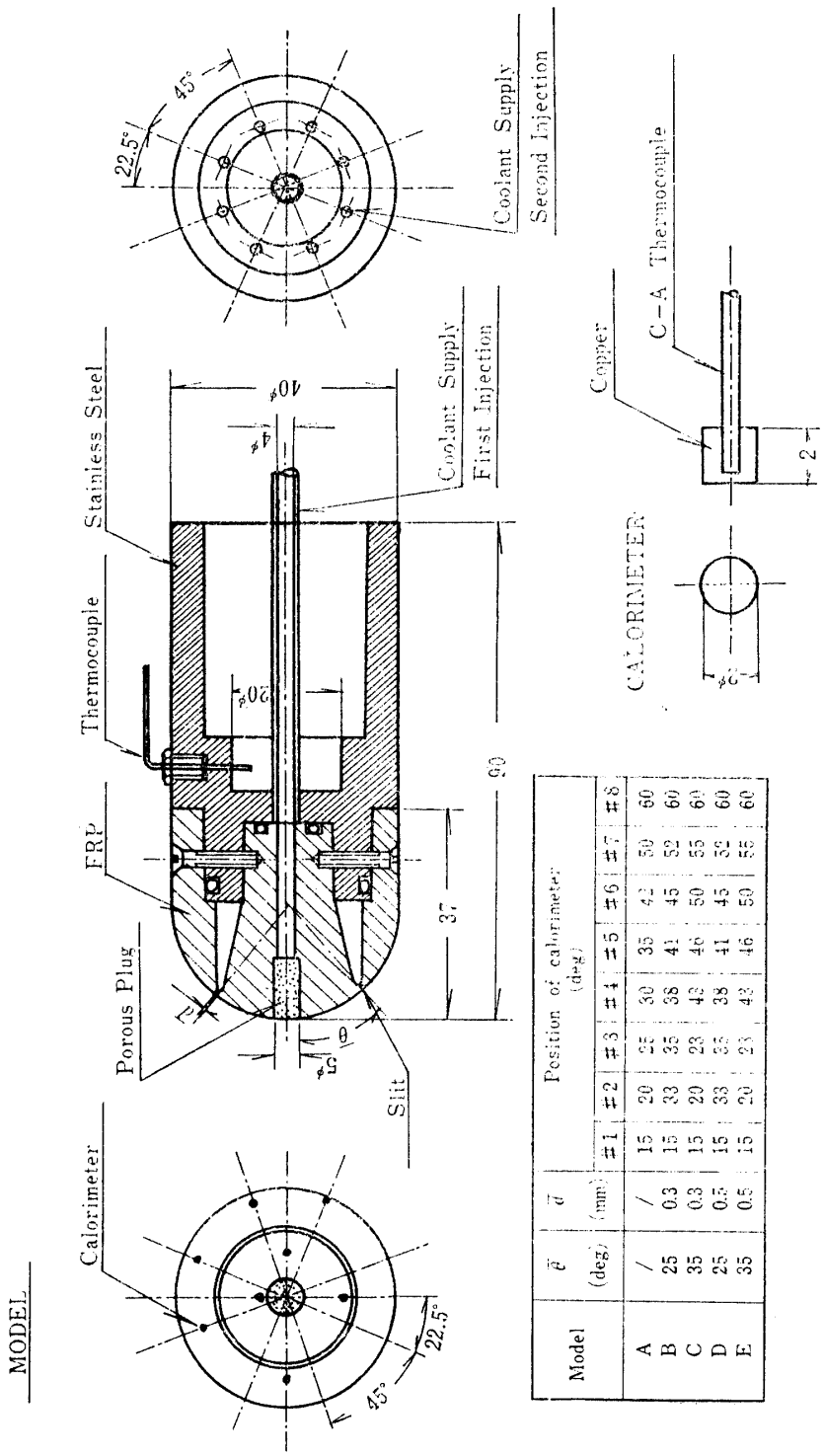

Model	θ (deg)	d (mm)	Position of calorimeter (deg)							
			#1	#2	#3	#4	#5	#6	#7	#8
A	/	/	15	20	25	30	35	42	50	60
B	25	0.3	15	33	35	38	41	45	52	60
C	35	0.3	15	20	23	43	46	50	55	60
D	25	0.5	15	33	35	38	41	45	52	60
E	35	0.5	15	20	23	43	46	50	55	60

Fig. 22. Experimental model.

$$\bar{T}_w(\bar{t}) = \bar{a} \exp(-\bar{b}\bar{t}) + \bar{T}_{eq}, \qquad (7\text{–}2\text{–}1)$$

and the three unknowns $(\bar{a}, \bar{b}, \bar{T}_{eq})$ were obtained by use of the measured temperature $\bar{T}_w(\bar{t})$ at $\bar{t}=70$, 80 and 90 seconds.

The current investigations have shown that the coolants having larger specific heats and less molecular weights are more effective to reduce the heating rate and the present experiment also shows the same trend, so that the data of the adiabatic wall temperature obtained by use of air injection were compared with the numerical calculations and the results are shown in Fig. 9(a) and Figs. 10(a) to (d). It is seen that the error between numerical and experimental results is about 10%, while qualitative agreement seems to be fairly good.

It is remarkable in Fig. 10(b) that existence of the second injection has no serious influence on the upstream data. This experimental fact seems to confirm the characteristics of the solution of the boundary layer equations of parabolic type indicated by the numerical results.

8. Conclusion

As a heat-shielding device for an axisymmetric blunt nosed bodies at hypersonic reentry, the method of local mass injection cooling at multiple stations was investigated and its cooling effectiveness was discussed in connection with a numerical approach to the boundary layer flows with discontinuous boundary conditions.

For the purpose of obtaining the applicable difference method appropriate to the modes of given discontinuity, one-dimensional heat conduction equation, which is of parabolic type as well as the boundary layer equations, was solved by means of the Hartree-Womersley method under the boundary conditions with several modes of discontinuity, and an appropriate difference method to give accurate approximation in the vicinity of the discontinuity was presented.

It was shown that common use of 3-pt difference at regular point together with particular use of 2-pt difference in the very vicinity of the singular point is appropriate to obtain numerical solutions of the boundary layer equations with discontinuous boundary conditions. Moreover, it was emphasized that the difference just ahead of the singularity should correspond to the left-derivative while it should correspond to the right-derivative just aft of the singularity.

Based on these arguments, an appropriate difference method was applied for an isothermal and an adiabatic wall conditions and the following results were obtained in connection with mass injection parameters such as total coolant mass flow and geometrical configuration of the coolant exit.

(1) The small coolant mass flow rate is rather favorable in the sense of the overall cooling effectiveness.

(2) Position of the exit is especially important, and the downstream injections should be appropriately located in the upstream vicinity of the peak point of the adiabatic wall temperature or the heat transfer distributions.

(3) If the total mass flow is kept constant, the effect of width of the exit is not so large.

An experiment made under the adiabatic wall conditions indicates fairly good qualitative agreement with the numerical results.

Comparison with the cooling effectiveness of the transpiration cooling showed that the local mass injection is more effective under the condition of the same coolant mass flow.

Acknowledgement

The author would like to express his deep thanks to Prof. R. Kawamura and Prof. K. Karashima for their cordial advices and instructive comments upon this work. The author also wishes to thank Mr. K. Sato for his valuable advices on the experiment.

Department of Aerodynamics
Institute of Space and Aeronautical Science
University of Tokyo, Tokyo
January 25, 1971

References

[1] McMahon, H. M.: "An Experimental Study of the Effect of Mass Injection at the Stagnation Point of a Blunt Body," California Institute of Technology, Guggenheim Aeronautical Lab., Hypersonic Project Memo. 42, 1958.
[2] Warren, C. H. E.: "An Experimental Investigation of the Effect of Electing a Coolant Gas at the Nose of a Bluff Body," Jour. Fluid Mech. 8, 400–417, 1960.
[3] Libby, P. A.: "The Homogeneous Boundary Layer at an Axisymmetric Stagnation Point with Large Rates of Injection," Jour. Aerospace Sci. 29, 48–60, 1962.
[4] Fox, H. and Libby, P. A.: "Helium Injection into the Boundary Layer at an Axisymmetric Stagnation Point," Jour. Aerospace Sci. 29, 921–934, 950, 1962.
[5] Kubota, T. and Fernandez, F. L.: "Boundary-Layer Flows with Large Injection and Heat Transfer," AIAA Jour. 6, 22–28, 1968.
[6] Derienzo, P. and Pallone, A. J.: "Convective Stagnation-Point Heating for Re-entry Speeds up to 70,000 fps Including Effects of Large Blowing Rates," AIAA Jour. 5, 193–200, 1967.
[7] Laganelli, A. L.: "A Comparison between Film Cooling and Transpiration Cooling System in High Speed Flow," AIAA Paper No. 70–153, 1970.
[8] Gollnick, Jr., A. F.: "Thermal Effects on a Transpiration Cooled Hemisphere," Jour. Aerospace Sci. 29, 583–590, 595, 1962.
[9] Goodwin, G. and Howe, J. T.: "Recent Developments in Mass, Momentum, and Energy Transfer at Hyper-Velocities," NASA SP 24, 1962.
[10] Swann, R. T. and South, J.: "A Theoretical Analysis of Effects of Ablation on Heat Transfer to an Arbitrary Axisymmetric Body," NASA TND 741, 1961.
[11] Steg, L. and Lew, H.: "Hypersonic Ablation," The High Temperature Aspect of Hypersonic Flow, Pergamon Press, 629–680, 1964.
[12] Karashima, K. and Kubota, H.: "Aerodynamic Study of Stagnation Ablation," Inst. Space and Aero. Sci., University of Tokyo ISAS Report 413, 1967.
[13] Karashima, K., Kubota, H. and Sato, K.: "An Aerodynamic Study of Ablation Near

the Region of Stagnation Point of Axially Symmetric Bodies at Hypersonic Speeds," Inst. Space and Aero. Sci., University of Tokyo, ISAS Report 425, 1968.

[14] Pallone, A.: "Nonsimilar Solutions of the Compressible-Laminar Boundary-Layer Equations with Applications to the Upstream-Transpiration Cooling Problem," Jour. Aerospace Sci. 28, 449–492, 1961.

[15] Rheinboldt, W.: "On the Calculation of Steady Boundary Layers for Continuous Suction, with Discontinuously Variable Suction Velocity," NASA TT F 29, 1961.

[16] Devan, L.: "Approximate Solution of the Compressible Laminar Boundary-Layer Equations," AIAA Jour. 6, 2010–2012, 1968.

[17] Morduchow, M. and Libby, P. A.: "Class of Solution of the Axisymmetric Boundary-Layer Equations with Mass Transfer," AIAA Jour. 6, 2045–2046, 1968.

[18] Bethel, H. E.: "Approximate Solution of the Laminar Boundary-Layer Equations with Mass Transfer," AIAA Jour. 6, 220–224, 1968.

[19] Hartree, D. R. and Womersley, J. R.: "A Method for the Numerical or Mechanical Solution of Certain Types of Partial Differential Equations," Proc. Royal Soc. 161A, 353–366, 1937.

[20] Smith, A. M. O. and Clutter, D. W.: "Solution of the Incompressible Laminar Boundary-Layer Equations," AIAA Jour. 1, 2062–2071, 1963.

[21] Smith, A. M. O. and Clutter, D. W.: "Solution of Prandtl's Boundary-Layer Equations," Douglas Aircraft Co., Engineering Paper 1530, 1963.

[22] Clutter, D. W. and Smith, A. M. O.: "Solution of the General Boundary-Layer Equations for Compressible Laminar Flow, Including Transverse Curvature," Douglas Aircraft Co., Rept. LB 31088, 1968.

[23] Smith, A. M. O. and Clutter, D. W.: "Machine Calculation of Compressible Boundary Layers," AIAA Jour. 3, 639–647, 1965.

[24] Jaffe, N. A., Lind, R. C. and Smith, A. M. O.: "Solution to the Binary Diffusion Laminar Boundary-Layer Equations with Second-Order Transverse Curvature," AIAA Jour. 5, 1563–1569, 1967; also Douglas Aircraft Co., Rept. LB 32613, 1966.

[25] Blottner, F. G.: "Chemical Nonequilibrium Boundary Layer," AIAA Jour. 2, 232–240, 1967.

[26] Fay, J. A. and Kaye, H.: "A Finite Difference Solution of Nonequilibrium Boundary Layers," AIAA Jour. 5, 1949–1954, 1967.

[27] Marvin, J. G. and Sinclare, A. R.: Convective Heating with Large Favorable Pressiure Gradient," AIAA Jour. 5, 1940–1948, 1967.

[28] Hayes, W. D. and Probstein, R. F.: "Hypersonic Flow Theory," Academic Press, Inc., 1960.

[29] Richtmyer, R. D. and Morton, K. W.: "Difference Methods for Initial-Value Problems," Second Edition, Interscience, 1967.

[30] Hilsenrath, J., et al.: "Tables of Thermal Properties of Gases," National Bureau of Standards, Circular 564, Nov. 1, 1955.

[31] Nachtsheim, P. R. and Swigert, P.: "Satisfaction of Asymptotic Boundary Conditions in Numerical Solution of Systems of Nonlinear Equations of Boundary-Layer Type," NASA TND 3004, 1965.

[32] Jaffe, N. A.: Private communication.

[33] Lees, L.: "Laminar Heat Transfer Over Blunt-Nosed Bodies at Hypersonic Flight Speeds," Jet Propulsion, 26, 259–269, 274, 1956.

[34] Gollnick, Jr., A. F.: "Blunt Body Experiments with Central Injection," AIAA Jour. 4, 374–376, 1966.